Simulation of gas channel temperatures during transients for SGT-800

LUND UNIVERSITY

Tobias Johansson

Thesis for the Degree of Master of Science
Division of Thermal Power Engineering
Department of Energy Science
Lund Institute of Technology | Lund University

Simulation of gas channel temperatures during transients for SGT-800.

Tobias Johansson
June 2016, Lund

Thesis for the degree of Master of Science in Engineering

Preface

This thesis constitutes the final part in achieving the degree of Master of Science in Mechanical Engineering. The project was conducted at the performance department at Siemens Industrial Turbomachinery in Finspång, Sweden.

I am grateful to a great many people who have contributed and supported me during this project and the list would be very long if I were to mention you all.

Tobias Johansson

"Success is not final, failure is not fatal: it is the courage to continue that counts."
- Winston Churchill

Abstract

Siemens Industrial Turbomachinery has developed dynamic gas turbine models to compute performance parameters such as temperature, pressure, mass flow and power during transients. Results from the current dynamic model correspond to measured data except for gas channel temperatures that change too fast during transients. The measurement of gas channel temperature is also a source of error due to the fact that probe temperature is measured instead of desired real temperature in the gas channel. It is of great interest to be able to simulate both real and probe temperatures in the gas channel to ensure that customer and development projects receive correct data.

The objective of this thesis is to implement heat soak to the existing dynamic gas turbine model of Siemens SGT-800. Probe models that compute temperature in probes at all cross sections along the gas channel were implemented to the existing gas turbine model.

A general method to calculate heat soak in gas turbines was discovered from literature and its reliability was proven by in-house reports. The method to calculated heat soak was implemented to SITs existing dynamic gas turbine model of Siemens SGT-800. When the heat soak model had been applied to the existing dynamic gas turbine model in Dymola and it was running in a correct way, the model was compared to measured data to ensure its agreement. To tune in the difference in gas channel temperature between measured data and the gas turbine model, parameters such as thermal mass, area and heat transfer coefficient were changed in the heat soak model. To emulate the inertia in the probe that occurs due to the metal encapsulation of the thermocouple, a transfer function was implemented. The probe inertia was tuned in towards measure data.

Implementing heat soak and probe inertia to gas channel temperatures in the gas turbine model resulted in good agreement to measured data during start operations. During stop and trip operations the gas channel temperature reacted too fast in the gas turbine model and further work is recommended. An additional thermal mass which is affected by a lower temperature might contribute to integrating inertia to the gas channel temperature. The mass flow during barring speed is different for measured data and the dynamic gas turbine model during stop and trip operations. Mass flows during barring speed and its effect on gas channel temperatures need further investigation.

Sammanfattning

Siemens Industrial Turbomachinery har tagit fram dynamiska gasturbinmodeller för att kunna beräkna prestandaparameterar såsom temperaturer, tryck, massflöden och effekt under transienter. Dagens modeller stämmer bra med uppmätt data med undantag för temperaturerna i gaskanalen, vilka reagerar för snabbt vid transienter. Temperaturmätningen i gaskanalen är även den en källa till fel, eftersom den inte mäter den verkliga lufttemperaturen, utan snarare temperaturen i mätsonden. Att kunna simulera den verkliga temperaturen i gaskanalen men även temperaturen i sonden är av stort värde för att kunna leverera korrekt data till kunder och utvecklingsprojekt.

Målet med examensarbetet är att ta fram en värmelagringsmodell till den redan befintliga dynamiska gasturbinmodellen av SGT-800. Sondmodeller som beräknar temperaturen i sonder ska även implementeras till den befintliga gasturbinmodellen, modellen ska kunna användas i alla snitt i gaskanalen.

En generell beräkningsmodell för värmelagring togs fram med hjälp från litteratur och dess korrekthet säkerställdes med hjälp av en intern rapport från SIT. Beräkningsmodellen implementerades till SIT:s befintliga dynamiska gasturbin modell av SGT-800. När modellen kunde köras, jämfördes den med uppmätt data för att utvärdera dess överstämmelse. För att trimma in skillnader mellan uppmätt data och gasturbinmodellen ändrades parametrar som termiska massa, area och värmeövergångstalet i värmelagringsmodellen. För att efterlikna trögheten i sonder som uppstår på grund av termoelementets inkapsling i metall implementerades en överföringsfunktion. Sondtrögheten trimmades in mot uppmätt data.

Implementering av värmelagring och sondtröghet ger en god överstämmelse för gaskanalstemperaturer mot uppmätt data under start. Under stopp och tripp reagerar gaskanaltemperaturen i gasturbinmodellen för snabbt och vidare arbete bör genomföras. Addera en ytterligare termisk massa som exponeras av en kallare temperatur kommer troligen integrera ytterligare tröghet till gastemperaturen i gaskanalen. Massflödena under barring varvtal skiljer sig mellan gasturbinmodellen och uppmätt data under stopp och tripp. Massflöde under barring varvtal och dess effekter på temperaturer i gaskanalen behöver utvärderas ytterligare.

Nomenclature

Latin symbols

A	$[m^2]$	Area
C	$[m]$	Chord length
c	$[m/s], [KJ/kgK]$	Velocity, Specific heat
c_p	$[KJ/kgK]$	Specific heat at constant pressure
c_v	$[KJ/kgK]$	Specific heat at constant volume
d	$[m]$	Diameter
e	$[J/(s \cdot m^2)]$	Energy radiated per unit area and unit time
F	$[N]$	Force
G	$[-]$	Gain
H	$[W]$	Enthalpy per time
HTC	$[W/m^2K]$	Heat transfer coefficient
h	$[J]$	Enthalpy
k	$[W/(mK)]$	Thermal conductivity
L	$[m]$	Length
m	$[kg]$	Mass
$\dot{m}$	$[kg/s]$	Mass flow
Nu	$[-]$	Nusselt number
n	$[-]$	Number of blades/vanes
p	$[Pa]$	Pressure
Pr	$[-]$	Prandtl number
Q	$[W]$	Heat transfer
q	$[W/m^2]$	Heat flux
Re	$[-]$	Reynolds number
r	$[m]$	Radius
T	$[K],[-]$	Temperature, Time constant
t	$[s],[m]$	Time, Thickness
U	$[m/s], [J],[-]$	Blade speed, Internal Energy, Input
u	$[m/s]$	Velocity
V	$[m^3]$	Volume
W	$[J]$	Work
x	$[m],[-]$	Length, Direction
Y	$[-]$	Output
y	$[-]$	Direction

Greek symbols

Δ	[-]	Difference
δ	[m]	Thermal boundary layer thickness
ε	[-]	Emissivity
μ	[Kg/(s·m)]	Dynamic viscosity
v	[m^2/s]	Kinematic viscosity
ρ	[Kg/m^3]	Density
σ	[W/(m^2 · K^4)]	Stefan-Boltzmann constant
τ	[Nm]	Torque
Ω	[rad/s]	Angular velocity

Subscripts

C	Compressor
c	Coefficient
d	Hydraulic diameter
f	Fluid
h	Hydraulic
ref	Reference
t	Thickness
W	Wall
x	Direction
θ	Tangential
∞	Surrounding fluid

Contents

1 Introduction

For more than 300 years Finspång mill was one of Europe's leading centers for cannon production [1]. The De Geer family was in charge of the factory for two centuries with the founder Louis De Geer as the leader of Swedish industry during a period of time. In the early years of the 20th century the Finspång mill was closed down and the estate was divided up into several pieces [2]. Two brothers who had just started their business in Stockholm saw the possibility in the location, the facilities and the craftsmanship in the area. They were Birger and Fredrik Ljungström, the founders of STAL (Svenska Turbinfabrik AB Ljungström) and they moved their recently set-up business to Finspång and continued their production of steam turbines in the new location. In 1953 STAL's first gas turbine was launched. Over the years there have been several company configurations but in 2003 Siemens acquired the business and formed Siemens Industrial Turbomachinery AB [3]. The main businesses at SIT are development, production and maintenance service of gas turbines. SIT are currently providing five gas turbine models in the range of 19 MW to 53 MW.

1.1 Background

One of our generation's greatest tasks is to handle the environmental challenges that the world stands in front of. Recently the world's leaders were gathered in Paris to negotiate the Paris agreement, a global agreement to reduce the climate change with several objectives and milestones until 2050 [4]. During recent years the willingness to invest in renewable source of energy has increased and new challenges have appeared, as how to handle renewable intermittent sources. Combining gas turbines with renewable intermittent sources is an effective way to avoid peak load shortage in the power grid.

The importance of transient behavior for gas turbines has increased during recent years due to high demand of gas turbines to handle load changes in efficient ways. SIT is at the forefront of the industrial gas turbine industry and the development of dynamic models of their gas turbines has been going on for more than 10 years. The objective is to recreate dynamic models with behavior as close as possible to real gas turbines. More detailed dynamic models have been developed and the influence of transient behavior due to heat soak has become more important [5]. Heat soak can be defined as heat exchange between components and gas flow depending on differences in temperature. It is especially noticeably at start, stop and fast load changes.

The purpose of dynamic models at SIT is to compute performance parameters as temperature, pressure, mass flow and power during transients. Results from the current dynamic model correspond to measured data except for gas channel temperatures that change too fast during transients [6]. The measurement of gas channel temperature is also a source of error due to the fact that probe temperature is measured instead of desired real temperature in the gas channel. It is of great interest to be able to simulate both real and probe temperatures in the gas channel to ensure that customer and development projects receive correct data.

1.2 Objectives

The objective of this thesis is to implement heat soak to the existing dynamic gas turbine model of Siemens SGT-800. Probe models that compute temperature in probes at all cross sections along the gas channel are also implemented to the existing gas turbine model.

1

1.3 Limitations

To ensure validity of the heat soak model comparison to real industrial data is necessary. As little useful measured data from different gas turbines stationed around the world have been publish, the general approach of the heat soak model has not been as thoroughly studied as desired. Extreme difference in ambient conditions and how the heat soak model reacts during such conditions have not been studied either.

Conduction has a certain impact in the casing, in the compressor- and in the turbine rotor. However, in this thesis conduction in metal components have been neglected due to its minor impact on heat soak.

A linear temperature relation was assumed during compression and expansion in the compressor and the turbine respectively. The temperature decreases or increases with the same amount for each stage in the compressor and the turbine.

The probe inertia was tuned in with a transfer function instead of implementing an additional heat soak model. This assumption was made due to the objective of this project, to save execution time. The correct temperatures in the gas channel were requested, not to construct a correct physical model of a gas turbine with its corresponding probes.

The cooling of turbine components was maintained as simple as possible, as it only impacts on temperatures in the gas channel. The average temperature in the gas channel with injected cooled air was computed.

1.4 Method

The project started with a literature study where articles, reports and in-house projects were evaluated for information and theory that could be applicable for this thesis. Heat transfer convection, heat storage in metal components and transient behavior in general for gas turbines were of main interest. A general method to calculate heat soak in gas turbines was discovered from literature [7] and its reliability was proven from in-house reports [5] [8] [9]. The method to calculate heat soak was implemented to SITs existing dynamic gas turbine model of Siemens SGT-800. SIT currently uses the dynamic modeling and simulation tool Dymola to model and simulate dynamic behavior of their gas turbines.

Heat soak was applied to gas turbine components in the form of a compressor, a combustor and a turbine. To get a result as correct as possible heat soak for the three different parts was further divided up into smaller pieces. Heat soak for the compressor and turbine was applied for every stage, fifteen and tree stages respectively. Heat soak at the combustor was divided up into two different parts, a casing and a combustor area. A more correct gas temperature and heat transfer coefficient is the main cause of dividing the heat soak model into smaller parts. To get mass, area and heat transfer coefficients at a design point in the heat soak model as correct as possible, hand calculations, experience, knowledge and computer programs have supplemented each other.

When the heat soak model had been applied to the existing dynamic gas turbine model in Dymola and it was running in a correct way, the model was compared to measured data to ensure its agreement. The transients that were evaluated were a start, a stop and a trip. As expected a difference in gas channel temperature between measured data and the dynamic model appeared. To tune in the difference in gas channel

2

temperature, parameters such as thermal mass, area and heat transfer coefficient were changed in the heat soak model. To emulate the inertia in the probe that occurs due to the metal encapsulation of the thermocouple, a transfer function was implemented. Information about the probe inertia was limited and it was mainly tuned in towards measure data.

During this project continual support and assistance offered from other departments within the Siemens group has ensured the quality of the project as well as providing guidance in new areas of interest.

1.5 Outline of the thesis
A brief introduction to each of the chapters included in this thesis are provide below.

1.5.1 Chapter 1
The thesis starts with an introduction of company history and the background of the object of study. Objectives and limitations are presented briefly. The first chapter ends with a brief explanation of how the project was conducted.

1.5.2 Chapter 2
The theory chapter contains the working principle of a generic gas turbine and a description of the SGT-800. The different methods and laws of heat transfer are explained. Dimensionless numbers and the heat transfer coefficient are described. The first order transfer function is derived and all software used in this project is explained.

1.5.3 Chapter 3
In the methodology chapter all steps that have been conducted during the project are stated. The configuration and implementation of the heat soak model in Dymola constitutes the largest part.

1.5.4 Chapter 4
All results are compiled in this chapter. The first part consists of charts illustrating the effect of changing the heat transfer coefficient and thermal mass to the gas channel temperature. The second part illustrates the implementation of heat soak and probe inertia into a gas turbine model.

1.5.5 Chapter 5
Results and problems which emerged during the project are accounted for. Conclusions are drawn in relation to earlier work and future work is suggested.

2 Theory

The gas turbine is one of the most important inventions of the 20th century and has had major impact in the energy industry. Gas turbines are widespread in many areas where power is needed to produce electricity, drive equipment or propel vehicles. Gas turbines are for example used in the energy industry to produce electricity, in the oil and gas industry to drive pumps and compressors, in propel aircrafts and in vessels. The application of gas turbines is often divided into two groups: industrial gas turbines and aero derivative gas turbines. Aero derivative gas turbines are of lighter construction and optimized to generate thrust from the exhaust gas. Industrial gas turbines are of heavier construction and more integrated to generate power from the shaft. This project is defined to industrial gas turbines.

2.1 Working principle of a gas turbine

A gas turbine configuration must comprise components such as a compressor, a combustor and a turbine. A schematic layout of a single shaft gas turbine is presented in figure 1 below. A configuration that includes these components is a simple cycle but other components as for example a re-heater can be added to increase the turbine power output. All configurations that includes more components then the basic three goes under the name of complex cycles.
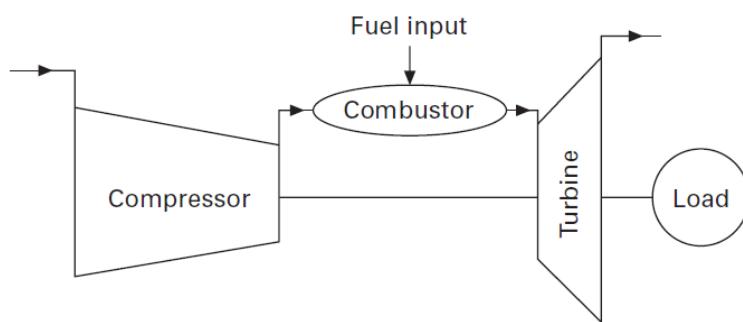
Figure 1 – Schematic layout of a single gas turbine.

Combining a steam cycle (Rankine) with a gas cycle (Bryton) is an efficient way to reach higher thermal efficient and has been a common configuration of new power plants. The exhaust gas leaves the gas turbine at a high temperature and the possibility to take care of the heat by transferring it to the steam cycle is an efficient way to increase the thermal efficiency.

Air at ambient condition flows through a compressor that compresses air to a higher pressure. The compressed air then enters a combustor where fuel is injected and ignited to generate a high temperature flow. The high temperature gas expands through the turbine to exhaust conditions to generate mechanical work to the rotating shaft.

For a turbine to generate power it needs a higher pressure at the inlet than at the outlet. The turbine work is used to drive the compressor and other devices as a generator. The power output from a gas turbine depends on the compressor, the combustor and the turbine efficiency. Higher efficiency in these components increases the power output and thermal efficiency.

4

An ideal gas turbine works as a Bryton cycle, which means that the gas undergoes three thermodynamic processes: an isentropic compression (1-2), an isobaric heat addition (2-3) and an isotropic expansion (3-4), as illustrated in figure 2 below [10].
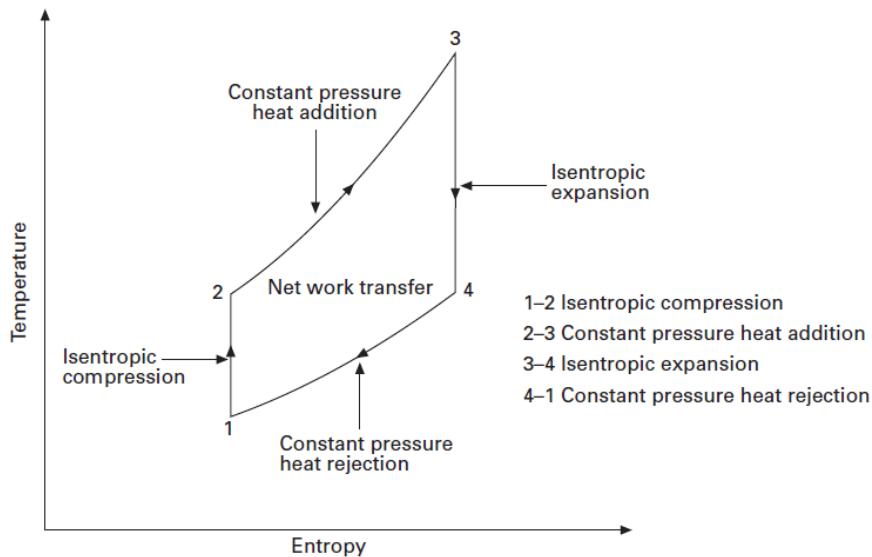

Figure 2 – T-s chart of an ideal simple cycle.

2.2 Single-shaft gas turbine and multi-shaft gas turbine

A gas turbine can be compiled in a variety of configurations that are adapted to different applications. To drive at a constant speed or continuously tune in the speed after an intermittent demand needs different types of machines.

As shown in figure 1 above, a single gas turbine consists of a compressor, a combustor and a turbine. The shaft connects the compressor and turbine. Thus, both the compressor and the turbine rotate at the same speed. The single shaft gas turbine is suited to fixed speed at base load power generation. An advantage with single shaft gas turbines is that the compressor prevents over-speed due to the detection of high power demand that occurs when speed increases.

In this project Siemens single-shaft gas turbine the SGT-800 is the object of study. Multi-shaft gas turbines are also explained to inform the reader about the difference. A multi-shaft gas turbine is split into two or more spools, as one can see in figure 3 below. The expansion is divided into turbines that drive the compressors and one that drives the load in terms of a power turbine. A multi-shaft gas turbine runs with good performance independently of the requested rotational speed or power of the load. Multi-shaft gas turbines are commonly used to drive loads as a mechanical drive application where rotational speed and power differ. A disadvantage with a multi-shaft gas turbine is the possibility for the power turbine of reaching over-speed.
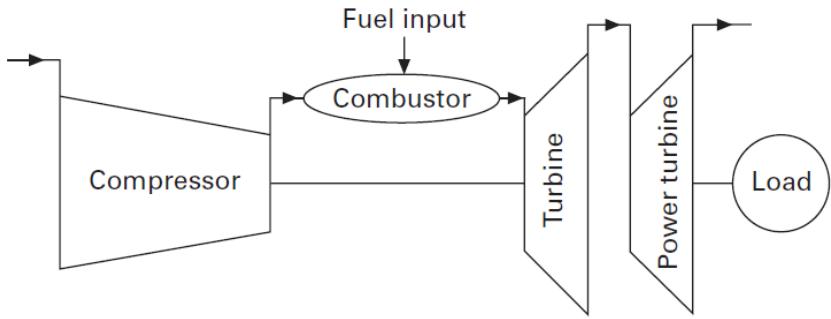
Figure 3 – Schematic layout of a multi-shaft gas turbine.

2.3 Euler work equation

To analyze the transferred energy in a gas turbine the momentum equation constitutes a vital role. The momentum equation describes the total force acting on the blades in a compressor or turbine cascade caused by deflection or acceleration of fluid passing the blades. From the equation below a system consisting of a mass m with all forces acting on m in an arbitrary direction describes the time rate of change of the total momentum. As explained earlier m is the system's mass, c_x and F_x are the velocity and the force respectively in the given direction.

$$\sum F_x = \frac{d}{dt}(m \cdot c_x) \tag{1}$$

Equation 2 describes the steady flow moment equation in one dimension.

$$\sum F_x = \dot{m}(c_{x2} - c_{x1}) \tag{2}$$

To describe the torque of all external forces acting on an arbitrary axis fixed in space the momentum equation could be further derived as in equation 3 where r is the distance from the axis center to the mass center from the axis of rotation measured along the normal and c_θ the velocity perpendicular to both the axis and the radius vector.

$$\tau_A = m \cdot \frac{d}{dt}(r \cdot c_\theta) \tag{3}$$

For one dimensional flow the equation is as follows.

$$\tau_A = \dot{m}(r_2 \cdot c_{\theta 2} - r_1 \cdot c_{\theta 1}) \tag{4}$$

6
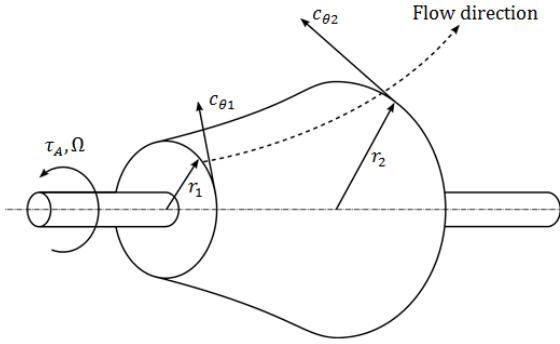
*Figure 4 – Control volume of a turbomachine.*

The amount of work the rotor does on the fluid in a compressor is explained by the Euler compressor equation. The equation is derived from the summation of the moment equation above and the blade speed $U = \Omega \cdot r$.

$$\dot{W}_c = \tau_A \cdot \Omega = \dot{m}(U_2 \cdot c_{\theta 2} - U_1 \cdot c_{\theta 1}) \tag{5}$$

The work per unit mass can be describe as

$$\Delta W_c = \frac{\dot{W}_c}{\dot{m}} = U_2 \cdot c_{\theta 2} - U_1 \cdot c_{\theta 1} \tag{6}$$

For a compressor this equation should have a lager value than zero.

For a turbine the fluid makes work on the rotor and thus the process is reversed to a compressor. The process is explained by Euler turbine equation.

$$\Delta W_c = \frac{\dot{W}_c}{\dot{m}} = U_1 \cdot c_{\theta 1} - U_2 \cdot c_{\theta 2} \tag{7}$$

The compressor- and turbine equations constitute the Euler work equation. The Euler equation is applicable for steady flow but is also valid for time-average unsteady flow [11].

2.4 SGT-800

The SGT-800 has currently the largest power output in Siemens Finspångs portfolio of industrial gas turbines. The development of the machine started in 1994 and it has since been one of the company's greatest sellers [12]. With an initial power output of 45 MW and an electric efficiency of 37 per cent. From the first unit several upgrades have been done during the years and today the SGT-800 is available in three ratings of 47.5 MW, 50.5 MW and 53.0 MW (2016) [13]. The SGT-800's robust design, low emissions and high efficiency makes it an attractive solution for many applications in energy production and cogeneration. The high exhaust gas temperature makes it an excellent choice for cogeneration and combined cycle applications [14]. The gas turbine can be delivered in two types of packages. The classic package and a single lift package which differs in that the single lift package has a lift capacity of the complete train consisting of gas turbine, gearbox, generator and mechanical auxiliary systems and therefor is more convenient for inaccessible places [14].

Figure 5 – The single lift package.

The SGT-800 is a single shaft gas turbine and the main components: compressor, combustor and turbine will be further explained.

A 15 stage axial compressor with three variable guide vanes provide the combustor with compressed air at a pressure ratio of 20:1 [15]. The compressor is equipped with five extractions providing compressed air to turbine blade cooling and bleed valves [15]. The bleed valve's task is to protect the compressor from stall and surge condition during start-up and shut-down.

The SGT-800 combustor consists of 30 burners placed in an annular design [14]. The combustor is of Siemens's third generation of dry low-emission combustors [13]. To reduce heat loss from the combustor the SGT-800 combustor is equipped with a convective cooling system complemented with a thermal barrier coating [15].

The SGT-800 is equipped with a three stage turbine where the first two stages of blades and vanes are cooled by air and the third stage is uncooled [13]. All three turbine disks are cooled and the first stage of blades and vanes has a film cooling system to protect the blades and vanes against entering high temperate gas [15].
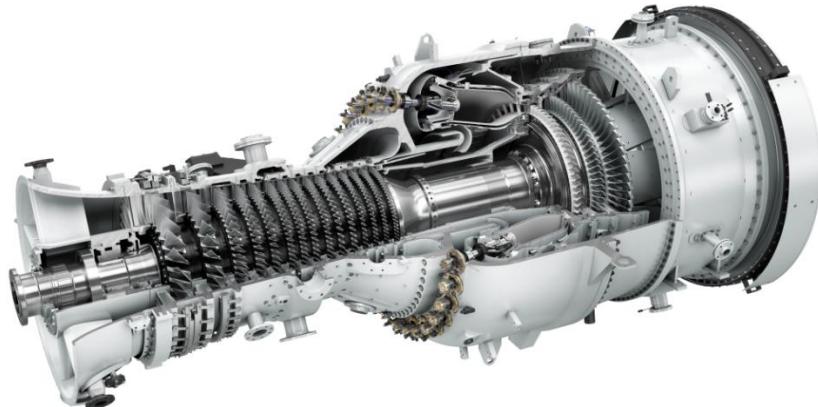

Figure 6 – SGT-800.

2.5 Heat transfer

Heat transfer occurs when there is a temperature difference between an area with higher temperature and another with a lower temperature. Heat always transfers from the warmer area to the colder one. The three fundamental physical processes of heat transfer are conduction, convection and radiation [16].

2.5.1 The first law of thermodynamics

The first law of thermodynamics has its origin in the law of conservation but is adapted to thermodynamic systems. The basic form of the first law of thermodynamics for a closed system is shown below and illustrated in figure 7.

$$Q = W + \frac{dU}{dt} \tag{8}$$

Q is the heat transfer rate, W is the transferred work and $\frac{dU}{dt}$ describes the rate of change of internal energy.
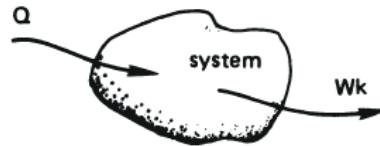
Figure 7 – A closed system where heat and work is transferred.

When $p \, dV$ is the only work occurring, the basic version form of the first law of thermodynamics could be rewritten as

$$Q = p \frac{dV}{dt} + \frac{dU}{dt} \tag{9}$$

This equation could be written as two different cases depending on if the process is during constant pressure or volume.

Constant volume:

$$Q = \frac{dU}{dt} = m \cdot c_v \cdot \frac{dT}{dt} \tag{10}$$

Constant pressure:

$$Q = \frac{dh}{dt} = m \cdot c_p \cdot \frac{dT}{dt} \tag{11}$$

h is the enthalpy and c_v and c_p is the specific heat at constant volume and constant pressure respectively.

During an incompressible process the two specific heats are equal and the equation could be described as

$$Q = \frac{dU}{dt} = m \cdot c \cdot \frac{dT}{dt} \tag{12}$$

9

To define heat transfer the first law of thermodynamics must be complemented with Fourier's law to describe conduction, Newton's law of cooling to describe convection and Stefan-Boltzmann's law to describe thermal radiation. These equations will be explained later.

2.5.2 Conduction

Conduction is the energy transfer that occurs between particles with higher energetic level to particles with lower energetic level in a substance [17]. The phenomenon could be explained in a more refined way as molecules with a higher temperature also have a higher energy and when molecules with different energies collide a transfer of energy occurs from the more energetic to the less energetic molecules.

Fourier's law expresses an exposition of the theory of conduction. For a one dimensional system Fourier's law is expressed from equation 13 where q is the heat flux, the constant k is thermal conductivity and T is the temperature of the body. The thermal conductivity depends on both the position and temperature but is often assumed to be constant.

$$q = -k\frac{dt}{dx} \tag{13}$$

The three dimensional form of Fourier's law has the appearance as one can see below where q is now specified in direction and magnitude.

$$\vec{q} = -k\nabla T \tag{14}$$

As there is limited space in this thesis a brief introduction to conduction is presented. Further derivation of Fourier's law can be found in [18].

2.5.3 Convection

Heat transfer by convection consists of two different physical processes in terms of diffusion and bulk motion of the fluid [17]. Diffusion is heat transfer that occurs from molecule motion and was described earlier as conduction. Bulk motion temperature is heat transfer that occurs when a large amount of molecules is moving collectively. In the moving fluid molecules retain their random motion and therefore convection is a combination of heat transfer from fluid motion and molecular diffusion.

When a fluid enters a body of a different temperature the fluid forms a thin region nearest the body called a boundary layer [18]. Heat is transferred into the layer and sweeps through the boundary layer to the end where it again reverses into the stream. This process is called convection and is illustrated in figure 8 below.
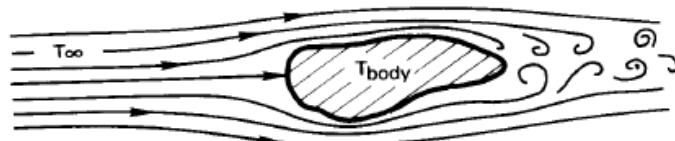

Figure 8 – Illustration of convection.

Newton managed to express the convective process of cooling as

$$\frac{dT_{body}}{dt} \propto T_{body} - T_\infty \tag{15}$$

Combining First law of thermodynamics with equation 15 gives

$$Q \propto T_{body} - T_\infty \tag{16}$$

This equation can be rephrased as Newton's law of cooling

$$Q = HTC \cdot A \cdot \left(T_{body} - T_\infty\right) \tag{17}$$

where Q is the rate of heat transfer, HTC is the heat transfer coefficient, A is the area exposed to heat transfer. T_{body} is the temperature of the body and T_∞ is the temperature of the fluid. The heat transfer coefficient depends on the condition in the boundary layer as surface geometry, fluid characteristics and fluid velocity.

Heat transfer by convection can be divided into two groups depending on the nature of the flow [17]. If the flow is caused by an external source as a fan or a pump the heat transfer is called forced convection. Natural convection occurs from natural sources often caused by density difference and by temperature variations in the fluid.

2.5.4 Radiation
Thermal radiation transfers energy with electromagnetic waves. The emission occurs from a body, liquid or gas due to changes in electron configurations [17]. In comparison to conduction and convection radiation does not need any contact between mediums to transfer heat. The intensity of heat radiation depends on temperature and the surface characteristics of the body [18].

The dependents of temperature influence on heat flux energy from radiation of a black body were experimentally establish by Stefan [18] and thermodynamic explained by Boltzmann [18]. The Stefan-Boltzmann law is

$$e_b(T) = \sigma \cdot T^4 \tag{18}$$

where Stefan-Boltzmann constant is $\sigma = 5{,}670400 \cdot 10^{-8}\, W/m^2 \cdot K^4$ and T is the temperature. A real body's heat flux is less than a black body and therefore a configuration factor ε is applied.

$$e_b(T) = \varepsilon \cdot \sigma \cdot T^4 \tag{19}$$

The rate of heat transferred by radiation between two bodies is showed below

$$Q = A \cdot e_{b1} - A \cdot e_{b2} = A \cdot \varepsilon \cdot \sigma \cdot (T_1^4 - T_2^4) \tag{20}$$

2.5.5 Heat soak
Heat transfer due to difference in temperature between the working fluid and the metal components during transients is called heat soak. The inertia in the metal components creates the difference in temperature against the fast shifting working medium. Heat soak depends on thermal masses, geometric data and heat transfer coefficients. Heat soak influences the gas turbine performance in several ways. For instance, heat soak works from the casing during a hot start as an additional fuel that will push the compressor towards rotating stall and higher temperatures [7].

2.5.6 Reynolds number

Osborn Reynolds discovered the transition between laminar and turbulent flow in a tube from experiments [18]. The description of the boundary layer thickness could be shown as equation 21 where u_∞ is the velocity, ρ is the density, μ is the dynamic viscosity and x is the length.

$$\delta = \text{fn}(u_\infty, \rho, \mu, x) \tag{21}$$

From this statement two dimensionless pi-groups are developed where v is the kinematic viscosity and Re_x is the Reynolds number.

$$\frac{\delta}{x} = \text{fn}(Re_x) \qquad Re_x = \frac{\rho \cdot u_\infty \cdot x}{\mu} = \frac{u_\infty \cdot x}{v} \tag{22}$$

Reynolds number defines the ratio of inertial and viscous forces in a fluid [18]. A low Reynolds number where viscous forces are dominant gives a laminar flow. A High Reynolds number where inertial forces are dominant gives a turbulent flow.

2.5.7 Nusselt number

A thermal boundary condition occurs when there is a temperature difference between the stream and a stream-related body. The thermal boundary layer for a wall is shown in figure 9 below. To derive the Nusslet number an expression between heat transfer by conduction and convection for an arbitrary wall in a stream is set as

$$-k_f \frac{dT}{dy} = HTC(T_W - T_\infty) \tag{23}$$

where k_f is the conductivity of the fluid. Fourier's law could be used to describe the heat transfer between the fluid and the wall because there is no velocity in the direction of q nearest the wall. The equation could be further arranged as

$$\frac{\partial \left(\frac{T_W - T}{T_W - T_\infty} \right)}{\partial (y/L)} = \frac{HTC \cdot L}{k_f} = Nu_L \tag{24}$$

where L is the characteristic dimension of the body. Nusselt number describes the ratio of heat transfer by convection and conduction across the thermal boundary layer.
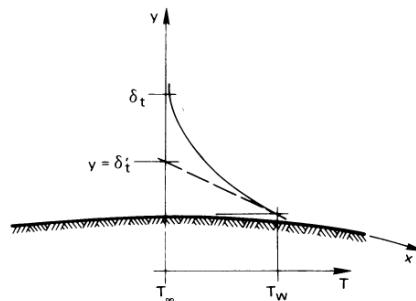

Figure 9 – Thermal boundary layer.

There is a strong connection between the thickness of the thermal boundary layer δ_t and Nusselt number illustrated in figure 9 above.

$$Nu = \frac{L}{\delta_t} \qquad (25)$$

2.5.8 Prandtl number

Prandtl number is a dimensionless parameter describing the ratio of diffusion of momentum to diffusion of heat in a fluid [19]. The Prandtl number depends only on the fluid and the fluid state and in many cases for gases it could be considered as a constant over a wide range of temperatures and pressures. Prandtl number is described as

$$Pr = \frac{\mu/\rho}{k_f/c_p \cdot \rho} = \frac{c_p \cdot \mu}{k_f} \qquad (26)$$

where μ is dynamic viscosity and k_f is the thermal conductivity.

2.5.9 Heat transfer coefficient

The heat transfer coefficient describes the ratio of heat flux to temperature difference between the fluid and the solid surface, as can be seen in equation 27 below [18].

$$HTC = \frac{Q}{T_w - T_\infty} \qquad (27)$$

Calculation of the heat transfer coefficient depends on several conditions as type of convection, heat transfer surface and fluid state. The heat transfer coefficient is often calculated from correlations based on dimensionless parameters such as Reynolds number, Prandtl number and Nusselt number [7]. The different correlations that have been used in the thesis to calculate Nusselt number and hence HTC are presented below.

Dittus-Boelter correlation

The Dittus-Boelter equation is tailored to force convection and turbulent flow in smooth tubes.

$$Nu = 0,021Re^{0,8}Pr^x \rightarrow HTC = \left(\frac{k}{d_h}\right)0,021Re^{0,8}Pr^x \qquad (28)$$

Kumada et. al's correlation

Kumada et. al studied the effect of the tip clearance on heat transfer on surfaces over the blade tip in an axial flow turbine [20]. The correlation can be used for estimate heat transfer coefficient over blades both in the compressor and turbine [21].

$$Nu = 0,052Re^{0,8}\left(1 - 2\bar{\delta}^{0,8}\right) \rightarrow HTC = \left(\frac{k}{C}\right) \cdot 0,052Re^{0,8}\left(1 - 2\bar{\delta}^{0,8}\right) \qquad (29)$$

where $\bar{\delta}$ is the relative tip clearance, the ratio between tip clearance and blade height. The characteristic dimension C is the cord length at the blade tip.

2.5.10 Transient scaling of the heat transfer coefficient

To derive the transient scaling factor a general expression for the Nusselt correlation for turbulent flow in a duct is presented.

$$Nu \sim Re_d^{0,8} \tag{30}$$

where the d is the hydraulic diameter.

Nusselt number is expressed as

$$Nu = \frac{HTC \cdot d}{k} \tag{31}$$

Combining equation 30 with equation 31 gives

$$HTC \sim \frac{k}{d} Re^{0,8} \tag{32}$$

The transient scaling factor for the heat transfer coefficient becomes

$$\frac{HTC(t)}{HTC_{ref}} = \frac{k(t) \cdot \left(\frac{\dot{m}(t)}{\mu(t)}\right)^{0,8}}{k_{ref} \cdot \left(\frac{\dot{m}_{ref}}{\mu_{ref}}\right)^{0,8}} \tag{33}$$

For the interval $300 - 800$ K, equation 34 and equation 35 are valid for air using exponential fitting to table data found in [22].

$$\mu \sim T^{0,71} \tag{34}$$

$$k \sim T^{0,79} \tag{35}$$

Implementing the expression for the dynamic viscosity and the thermal conductivity in equation 33 gives final expression for the transient scaling factor.

$$HTC(t) = HTC_{ref} \cdot \left(\frac{\dot{m}(t)}{\dot{m}_{ref}}\right)^{0,8} \cdot \left(\frac{T(t)^{0,79} \cdot T(t)^{-0,71 \cdot 0,8}}{T_{ref}^{0,79} \cdot T_{ref}^{-0,71 \cdot 0,8}}\right) \rightarrow$$

$$HTC(t) = HTC_{ref} \cdot \left(\frac{\dot{m}(t)}{\dot{m}_{ref}}\right)^{0,8} \cdot \left(\frac{\dot{T}(t)}{\dot{T}_{ref}}\right)^{0,22} \tag{36}$$

This scaling of the heat transfer coefficient is used for compressor and turbine.

Another way to scale the heat transfer coefficient is shown below

$$Nu = \frac{HTC \cdot L}{k} \tag{37}$$

$$Nu = 0{,}021 Re^{0{,}8} Pr^x \tag{38}$$

$$Re_x = \frac{\rho \cdot u_\infty \cdot x}{\mu} \tag{39}$$

Simplification of equations gives

$$HTC \sim \left(\frac{\dot{m}}{\mu}\right)^{0{,}8} \tag{40}$$

$$HTC(t) = HTC_{ref} \cdot \frac{k(t)}{k_{ref}} \cdot \left(\frac{\dot{m}(t)}{\dot{m}_{ref}}, \frac{\mu_{ref}}{\mu(t)}\right)^{0{,}8} \tag{41}$$

This method of scaling is used at the combustor [23].

2.6 First order transfer function
The derivative of a systems governing differential equation decides the order of the dynamic system. The general form of a first order differential equation is described as

$$T \cdot \dot{y}(t) + y(t) = G \cdot u(t) \tag{42}$$

where y is the response of the system, u is the input to the system, T is the time constant and G is the gain of the system.

A Laplace transformation of the first order system gives

$$T \cdot Y(s) + Y(s) = G \cdot U(s) \tag{43}$$

The transfer function gets the form of

$$Y(s) = \frac{G}{T \cdot s + 1} \cdot U(s) \tag{44}$$

2.7 Software
A compilation of computer programs has been used to model the dynamic behavior of heat soak, probe inertia and retrieve data for validation.

2.7.1 Dymola
Dymola is a tool for modeling and simulation of complex and integrated dynamic systems [24]. It is based on the Modelica language which is a free object-orientated modeling language. Modelica describes physical systems through equations instead of algorithms which makes the language more comprehensive and user-friendly. The user only needs to write equations which characterize the system and then Dymola or another Modelica based program translates the equation into an efficient code. In Dymola classes could be extended or used as an object and by combining objects, larger constellations are created. Dymola is equipped with a graphic editor which makes it possible to model just by drag and drop. Using drag and drop does not need any knowledge of the Modelica language and it is a convenient way to design models. The Modelica language gives the user the possibility to create their own component libraries or modify the already existing standard libraries [24]. The flexibility of Dymola makes it perfect for modeling and simulation of new technologies. Dymola

consists of two different environments in terms of a modeling and a simulation mode. The modeling environment has been described previously and in short terms is where the model is put together by equations. The simulation environment translates equations into efficient code and solves them. In the simulation environment there is also the possibility to visualize the dynamic behavior of the system due to time dependent graphs.
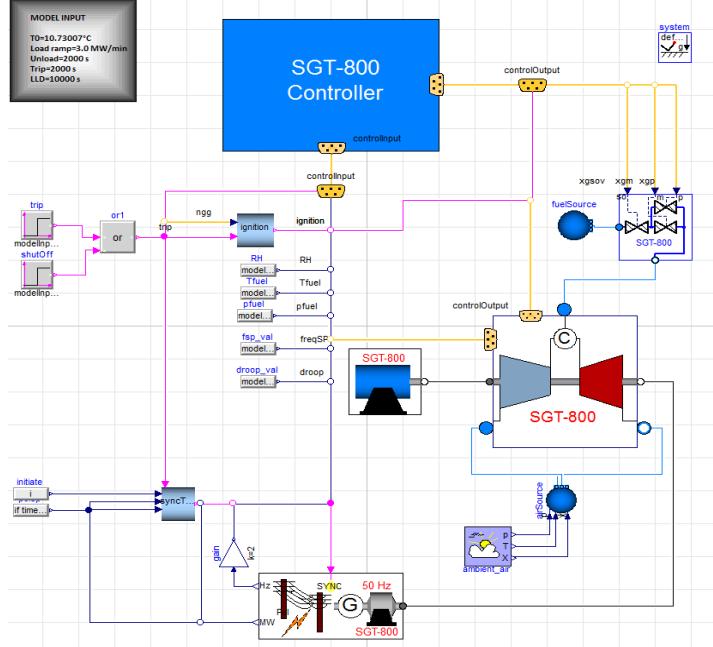
Figure 10 - Schematic figure of Siemens dynamic model of the SGT-800 in Dymola.

2.7.2 STA-RMS

STA-RMS (Siemens Turbomachinery Applications – Remote Monitoring System) is a platform that collects data from Siemens applications in areas as oil and gas, industrial and power generation [25]. The remote monitoring system collects and stores measurement data and alarms from site. The collected data are transferred to a central database where they are made available. The database consists of historic information in terms of raw data collected from equipment at site. With the RMSView tool the user can easily access performance parameters from the past for any machine in SIT's product portfolio. From a list the user can choose parameters that are of interest and make a chart consisting of several parameters during a specific time period. The parameters included in the chart can be exported to Excel for further work. Due to its advantages STA-RMS is an appreciated tool for product designers to statistical analysis product performance.

2.7.3 TeMas

TeMas is a database where data from various test performed by the R&D organization at Siemens Industrial turbomachinery in Finspång are compiled [26]. A tool to transfer data from the TeMas database is TeMas Export which exports data as a csv-file. TeMas Export gives easy access to requested data for a certain time period. TeMas also contains additional information to the executed tests as for example position of measurement points.

3 Methodology

In this section insight into the different procedures that have been executed during the project is given. It serves to provide an understanding of how the heat soak model was constructed and the decisions that were made during the project to form the end product.

The project started with a literature study where reports and articles were evaluated. Equations found in the literature were compiled and reviewed in order to constitute the base of the heat soak model. The heat soak model was modelled in Dymola and when it fulfilled the requested appearance the model was implemented to one of Siemens's existing dynamic models; the SGT-800. The model was compared to measured data and then tuned in with differing parameters from the heat soak model and adding probe inertia. Finally, the model was validated towards measured data from different sites.

3.1 Literature study

The literature study is the basis of the theory chapter and the purpose at the start of this project was to find a prior project that had implemented heat soak to a gas turbine, gain knowledge from it and contribute further to that knowledge. However, such a project could not be found, which suggests that there is a gap in the literature regarding the implementation of heat soak to a gas turbine. Consequently, the literature study changed its character to search for reports and articles and compile equations for the heat soak model. Later in the process the Siemens department in Montreal confirmed that correct equations had been used or at least the same as they use in their heat soak model. An idea of how to calculate heat soak in gas turbines is presented in Walsh & Fletcher [7]. The equation Walsh & Fletcher compile for calculating heat soak is shown below.

$$Q = HTC \cdot A \cdot \left(T_{gas} - T_{metal}\right) \tag{45}$$

$$\Delta T_{gas} = \frac{-Q}{\dot{m} \cdot cp_{gas}} \tag{46}$$

$$\frac{dT_{metal}}{dt} = \frac{Q}{m_{metal} \cdot cp_{metal}} \tag{47}$$

The first equation presented is Newton's law of cooling, the second equation is the energy balance equation and the third equation is the first law of thermodynamics. Basic heat transfer complemented with specific heat transfer for gas turbines during transients were studied and several simplifications and limitations were defined.

3.2 Basic equations of heat soak

The basic equations for heat soak are elementary and comprise four equations. The equations describe an arbitrary body in a stream exposed to forced convection. During transients when a difference in temperature occurs between the fluid and the body the temperature which enters the body leaves the body with a different temperature. The difference in fluid temperature depends on heat soak in metal components and is illustrated by the equations and figure 11 below.
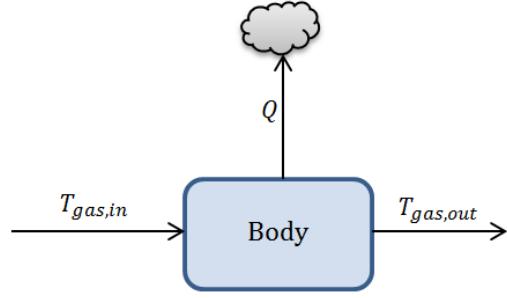
Figure 11 – Illustration of input and output in the heat soak model.

$$T_{gas} = \frac{T_{gas,in} + T_{gas,out}}{2} \qquad (48)$$

$$Q = HTC \cdot A \cdot \left(T_{gas} - T_{metal}\right) \qquad (49)$$

$$h_{gas,in} - h_{gas,out} - Q = 0 \qquad (50)$$

$$\frac{dT_{metal}}{dt} = \frac{Q}{m_{metal} \cdot cp_{metal}} \qquad (51)$$

An average temperature of the passing fluid is calculated with the first equation. The heat flow to or from the system is calculated with Newton's law of cooling. An energy balance equation for the system is described by the third equation. The first law of thermodynamics makes up the fourth equation and illustrates the metal temperature derivative. Geometric properties such as the surface area and the thermal mass could be calculated. The surface area is quite straight forward to calculate but the thermal mass is more demanding to determine because of the difficulties to know how much of the mass which is affected by heat transfer. Further explanation is described under limitations. The heat transfer coefficient is determined through correlations and is affected by changes in mass and temperature. The heat transfer coefficient needs a scaling factor during transients for better agreement. The specific heat of metal is considered constant.

3.3 Dymola model

The basis of the heat soak model consists of equations explained previously. To implement these equations into Dymola and make it work in an efficient way is explained in this section.

One of the objectives of this project was to preserve a reasonable execution time for the SGT-800 model in Dymola after heat soak was applied. The Dymola model should also accord with measured data. To achieve these criteria some simplifications were made. The heat soak model consists of three parts: the compressor, the combustor and the turbine. These parts were further divided into smaller pieces to get as accurate result as possible, but with responsible execution time. Dividing parts into smaller pieces affects several parameters to get more accurate as average fluid temperature in the gas channel and heat transfer coefficients.

3.3.1 Compressor model

Heat soak was applied to all fifteen stages in the compressor. It is illustrated in figures 16 and 17. Application of heat soak to each stage was decided on due to previous discussions according to a tradeoff between accuracy and execution time.

Heat soak for a stage

The basic model of heat soak at each stage is shown in figures 12 and 13 below. The input is the inlet and outlet air temperatures, temperature and mass rate for scaling the heat transfer coefficient and mass flow. From the code in figure 12 equations previously described and a scaling of the heat transfer coefficient define the heat soak model.

```
model heat_soak_stage_2

        parameter Modelica.SIunits.Area A;
        parameter Modelica.SIunits.Mass m_metal;
        parameter Modelica.SIunits.SpecificHeatCapacityAtConstantPressure cp_metal;
        parameter Modelica.SIunits.Temperature T_metal_start=288.15;
        parameter Modelica.SIunits.SurfaceCoefficientOfHeatTransfer HTC_ss;

        Modelica.SIunits.Temperature T_metal(start=T_metal_start);
        Modelica.SIunits.Temperature T_gas;
        Modelica.SIunits.SurfaceCoefficientOfHeatTransfer HTC;

equation
  T_gas=(T_gas_in + T_gas_out)/2;
  QU= HTC*A*(T_gas - T_metal);
  der(T_metal)=(QU)/(m_metal*cp_metal);
  HTC=HTC_ss*((mdot_gas_rate)^0.8)*((T_gas_out_rate)^0.22);

end heat_soak_stage_2;
```

Figure 12 – Code for the heat soak model at each stage.
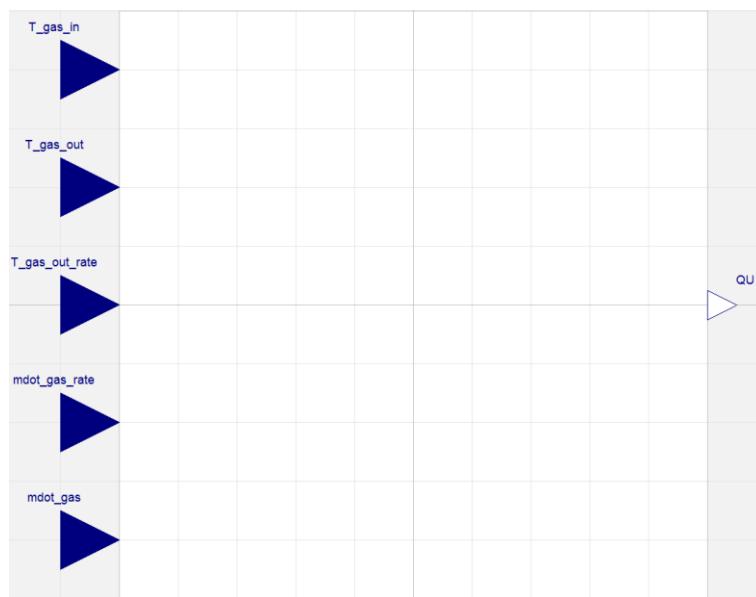
Figure 13 – Heat soak model at each stage.

Parameters can be changed at a specific stage by the user. A starting value is set for the metal temperature and should be changed according to ambient conditions. The specific heat in the compressor was obtained from a table. To determine the thermal mass, area and heat transfer coefficient for the compressor calculations were

conducted. Mass, surface area and heat transfer coefficients were computed with CAD and thermal state programs for the combustor and turbine parts.

Hub and tip radii were retrieved for both the leading and the trailing edges of each blade and vane to calculate the surface area. An average value for hub and tip radii was calculated.

$$r_{Hub} = \frac{r_{Hub,leading} + r_{Hub,traling}}{2} \tag{52}$$

$$r_{Tip} = \frac{r_{Tip,leading} + r_{Tip,traling}}{2} \tag{53}$$

The blade length is the difference between hub and tip radii.

$$L = r_{Tip} - r_{Hub} \tag{54}$$

Calculate blade area for blades and vanes in the compressor are shown in equation 55.

$$A_{Blade} = 2 \cdot n \cdot L \cdot C \tag{55}$$

n is the number of blades/vanes per stage and C is the chord length. The Chord length is illustrated by figure 14.
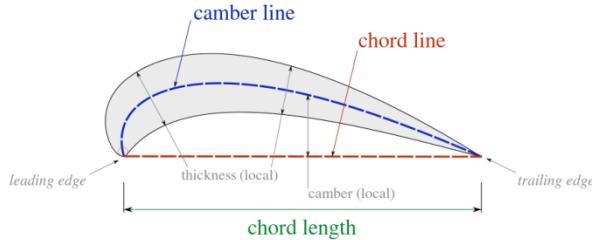
Figure 14 – Illustration of leading edge, trailing edge and chord length.

The platform area which will also be exposed to heat soak can be seen in figure 15. The calculation of the platform surface area was simplified due to the fact that the chord was used as the length of the platform.

$$A_{Platform} = 2 \cdot \pi \cdot r_{Hub} \cdot C \tag{56}$$

The definition of total area per stage.

$$A_{Stage} = A_{Blade} + A_{Platform} \tag{57}$$
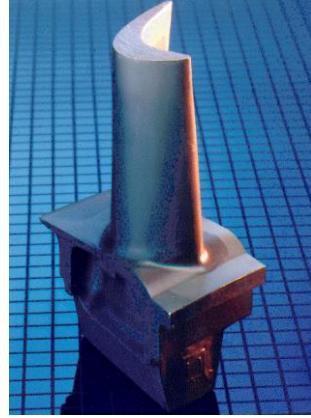
Figure 15 – Blade showing the platform.

Thermal mass was given for all blades and vanes but it needed to be calculated for the casing for both rotor and stator. To estimate the thickness of the casing that is exposed to heat transfer the value from an internal report at SIT was used: 20mm [8].

$$m_{Stator} = C \cdot \left(2 \cdot \pi \cdot r_{Tip}\right) \cdot t \cdot \rho \qquad (58)$$

$$m_{Rotor} = C \cdot (2 \cdot \pi \cdot r_{Hub}) \cdot t \cdot \rho \qquad (59)$$

From the equation above t is the thickness and ρ the density of the metal.

The total mass for each stage in the compressor is described as

$$m_{Stage} = m_{Blade} + m_{Vane} + m_{Stator} + m_{Rotor} \qquad (60)$$

Calculations were conducted in accord with an in-house report [21] at SIT to determine heat transfer coefficients at a reference case for the compressor. In the present project an average heat transfer coefficient at a reference case for every stage is desired. Heat transfer coefficients at a reference case are defined as

$$Re = Re_C \frac{\rho \cdot u_\infty \cdot d_h}{\mu} \qquad (61)$$

Re_C is Reynolds correction factor and d_h is the hydraulic diameter.

$$Pr = \frac{c_p \cdot \mu}{k} \qquad (62)$$

Nusselt number from the Dittus-Boelter correlation

$$Nu = 0,021 Re^{0,8} Pr^x \qquad (63)$$

Nusselt number from derivation

$$Nu = \frac{HTC \cdot d_h}{k} \qquad (64)$$

Combining equation 63 and 64 gives

$$HTC = \left(\frac{k}{d_h}\right) 0{,}021 Re^{0,8} Pr^x \qquad (65)$$

Heat transfer coefficients at a reference case were calculated for rotor and stator parts for all fifteen stages.

Heat soak model

Combining all fifteen heat soak models created for each stage gives the total heat soak to the compressor, see figure 17. From the Dymola model of SGT-800 the gas temperatures at inlet and at outlet of the compressor are known but not the temperature at each stage. An assumption is made that the temperature increases across all stages in the compressor and are set to the same value. The effect of modification in mass flow varies according to extractions for compressed air to bleed valves and turbine cooling. Change in mass flow has been introduced in the heat soak model where the five extractions are placed. The output of the model is the total heat flow that occurs between the compressed air and the metal components in the compressor.

According to figures 16 and 17 each stage is connected to each other. Accordingly, the entering temperature is the temperature that leaves the previous stage and has been exposed to heat soak from the previous stage. This configuration makes the model more accurate to a real gas turbine.
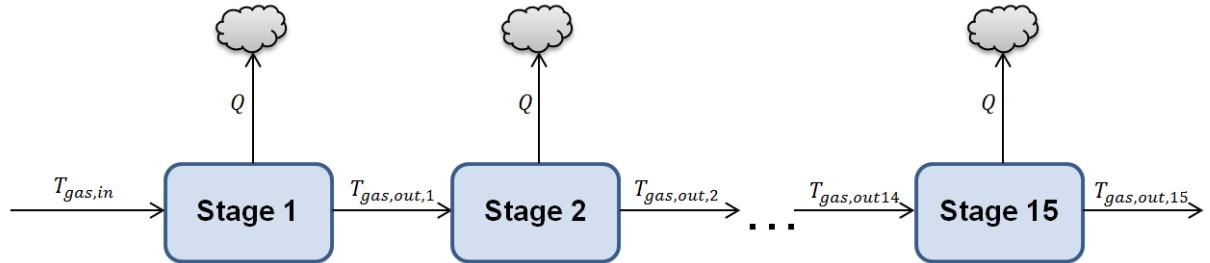
*Figure 16 – Illustration of the heat soak model of the compressor.*
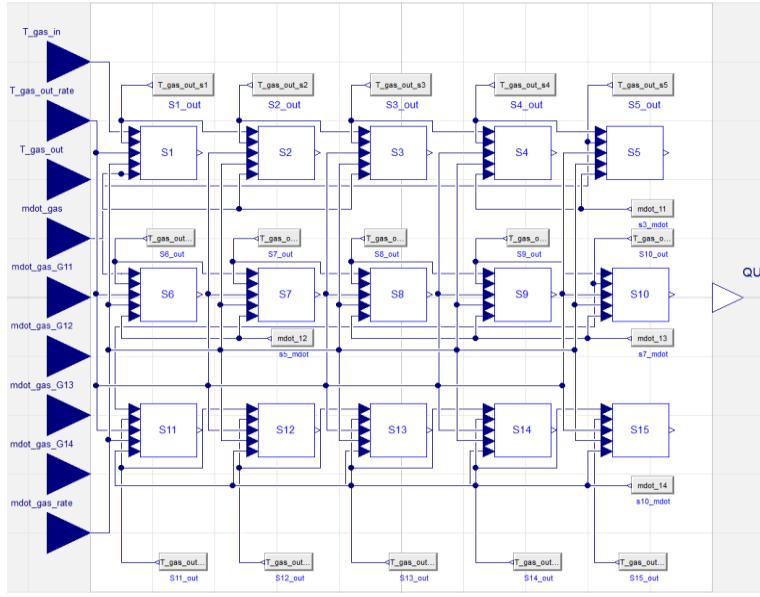
Figure 17 – Schematic picture of how the heat soak model in Dymola of the compressor is structured.

Implementation of heat soak model into compressor model

The heat soak model is implemented to the existing compressor model of the SGT-800 model in Dymola. The implementation of the heat soak model to the compressor is illustrated in figure 18. Inlet and output temperatures for the heat soak model are retrieved from the feed and drain port in the compressor model. Heat flow value computed from the heat soak model is implemented to the energy balance equation at the compressor.

$$H_{feed} - H_{drain} - Q = 0 \qquad (66)$$

Energy balance equation affects properties in ports which in turn affect the heat soak model. Mass flow and temperature parameters for scaling heat transfer coefficients were implemented in the compressor model. The scaling values were affected by several parameters such as ambient conditions. The ambient parameters are easily founded by simulate the model at steady state. To get properties in terms of mass flow and temperatures from the extractions to bleed valves and turbine blade cooling a medium is created in Dymola for each of the extractions. Energy flow and mass flow are added to the energy balance equation respectively, the mass balance equation for each of the five extractions.

23
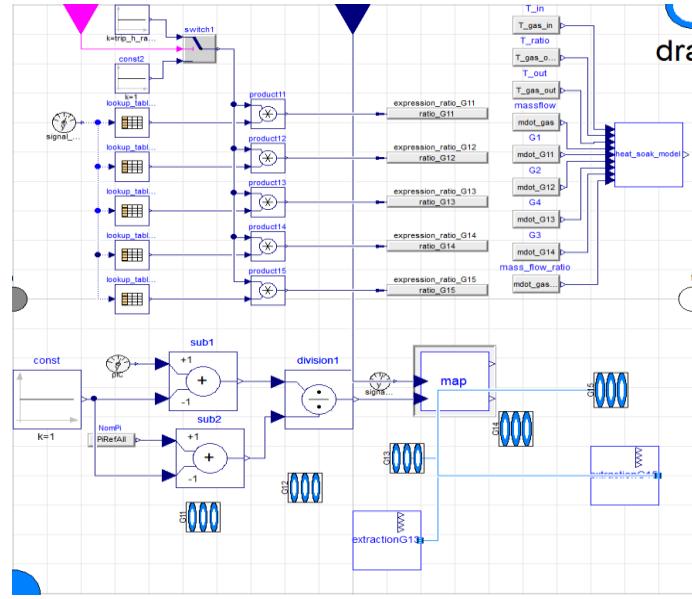
Figure 18 – Implementation of heat soak at compressor.

After heat soak was applied to the compressor an analysis was made where the influence of heat soak to gas channel temperatures were studied.

3.3.2 Combustor model

The heat soak model has been divided into two pieces in terms of a combustor part and a casing part. The casing consists of the metal that encapsulates the combustor. The combustor is exposed to high temperature and consists of a small area that makes the amount of heat soak in the metal restricted. The casing is exposed to lower temperature and consists of a large area where a large amount of energy can be stored. The combustor is directly exposed to the flame and heat transfers both through convection and radiation to the metal. As described previously in the theory chapter the combustor is equipped with a cooling system which neglects heat transfer to the casing through radiation. The casing part includes all metal that encapsulates the combustor beginning with the compressor diffusor. The casing part and combustor part are highlighted in figure 19.
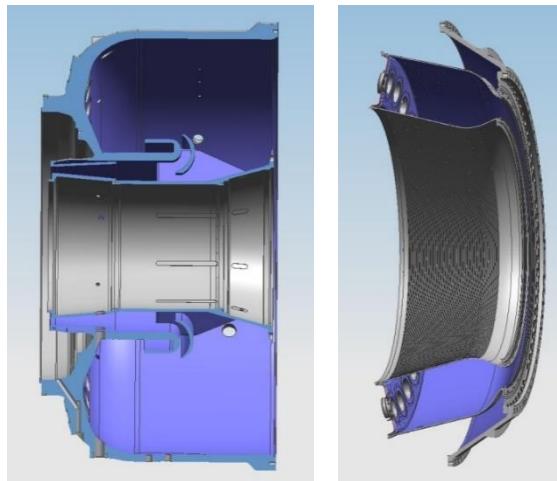
Figure 19 – Cross section of the casing and corresponding combustor.

24

Heat soak model for central casing and combustor

The basic heat soak model is structured in the same manner for all three different heat soak models. The heat soak model for the casing and combustor is illustrated in figure 20 below. The three basic equations constitute the model with a complementing equation for scaling heat transfer coefficient. The scaling process of heat transfer coefficient is simplified for the combustor and depending on mass flow only. This scaling method has been used in a report where heat transfer coefficients for the central casing were scaled [27].

$$T_{gas} = \frac{T_{gas,in} + T_{gas,out}}{2} \tag{67}$$

$$Q = HTC \cdot A \cdot \left(T_{gas} - T_{metal}\right) \tag{68}$$

$$\frac{dT_{metal}}{dt} = \frac{Q}{m_{metal} \cdot cp_{metal}} \tag{69}$$

$$HTC = HTC_{ref} \cdot \left(\frac{\dot{m}(t)}{\dot{m}_{ref}}\right)^{0,8} \tag{70}$$

Average air temperature in the central casing consists of inlet temperature that leaves the compressor and the temperature that enters the combustor. The average temperature of the combustor is also calculated where boundaries are easier to recognize.

Masses and areas for both central casing and combustor have been obtained from a CAD program, PTC creo. All of the surfaces that have been selected in the central casing and the combustor are highlighted in figure 19 above.

Specific heat has been obtained from a table for metal components in the central casing and the combustor.
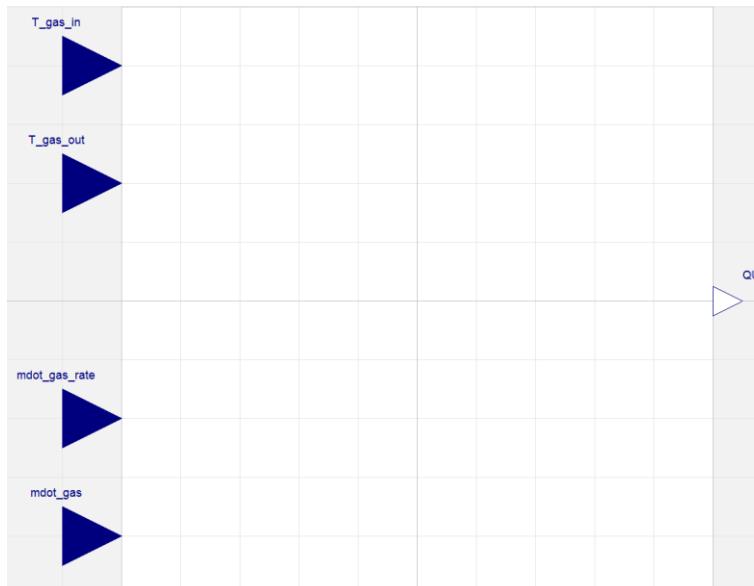

Figure 20 – Illustration of the basic heat soak model for the combustor and the central casing.

Calculations have been conducted according to an in-house code at SIT [23] to determine the heat transfer coefficient at a reference case of the combustor. The heat transfer coefficient at a reference case is defined as

$$Re = \frac{\rho \cdot u_\infty \cdot L}{\mu} \tag{71}$$

$$Pr = \frac{c_p \cdot \mu}{k} \tag{72}$$

Nusselt number from the Dittus-Boelter correlation

$$Nu = 0{,}021 Re^{0{,}8} Pr^x \tag{73}$$

Nusselt number from derivation

$$Nu = \frac{HTC \cdot L}{k} \tag{74}$$

Combining equation 73 and 74 gives

$$HTC = \left(\frac{k}{L}\right) 0{,}021 Re^{0{,}8} Pr^x \tag{75}$$

The result was compared to measured data with a satisfactory agreement. The heat transfer coefficient for the SGT-800 central casing was computed with a 2D thermal state program [27].

Heat transfer coefficients differ in the central casing for various areas. Areas with different heat transfer coefficients are described in figures 21 and 22.
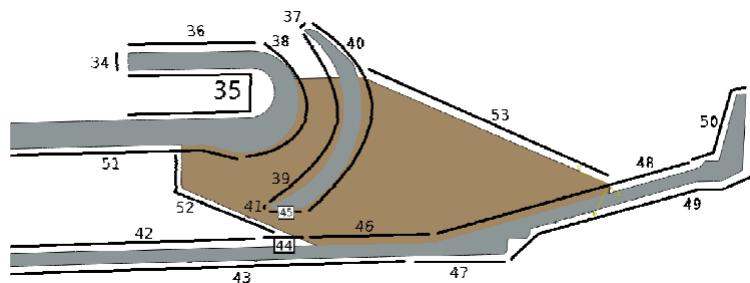
Figure 21 – Schematic picture of surfaces at the casing with a corresponding heat transfer coefficient.
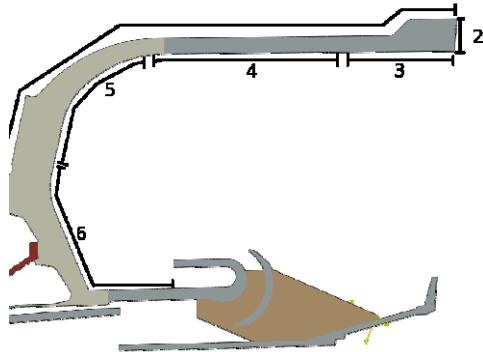
Figure 22 – Schematic picture of surfaces at the casing with a corresponding heat transfer coefficient.

To adapt the heat transfer coefficient to the heat soak model an average value for the heat transfer coefficient is needed. A fairly good value of the average heat transfer coefficient is obtained if a dependency of the area is implemented.

$$HTC_{casing,ref} = \frac{HTC_{1,ref} \cdot A_1 + HTC_{2,ref} \cdot A_2 + \cdots + HTC_{n,ref} \cdot A_n}{A_1 + A_2 + \cdots + A_n} \tag{76}$$

The heat transfer coefficient for a reference case is demanded for the combustor as well. The surfaces that are of interest are the heat shield and the inner liner. The relevant surfaces are indicated in figure 23 below. The heat transfer coefficient values at the two surfaces were defined by the finite element model [23]. The difference in the size of mesh in the two surfaces made it difficult to get a good average value. To get the average heat transfer coefficient value for the combustor influence of the area was applied.

$$HTC_{comb,ref} = \frac{HTC_{Heat\ shield,ref} \cdot A_{Heat\ shield} + HTC_{Inner\ liner,ref} \cdot A_{Inner\ liner}}{A_{Heat\ shield} + A_{Inner\ liner}} \tag{77}$$
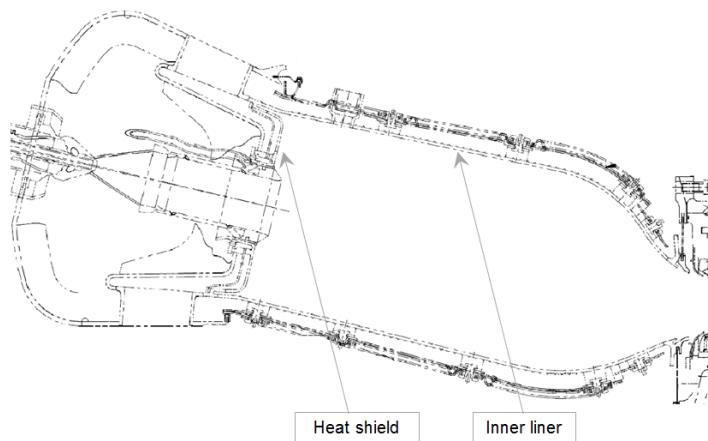

Figure 23 - Combustor surfaces.

Scaling of the reference heat transfer coefficient for the combustor was derived in the theory chapter. In the heat soak model a simplified scaling was chosen as the one used at the casing. The difference between the derived method and the simplified method is negligible.

$$HTC = HTC_{ref} \cdot \left(\frac{\dot{m}(t)}{\dot{m}_{ref}} \right)^{0,8} \tag{78}$$

Heat soak model

The heat soak model for the combustor consists of heat soak occurring in the central casing and in the combustor. The inlet temperature to the casing consists of compressed air leaving the compressor. The entering temperature to the combustor is air leaving the casing with heat soak applied. The output from the heat soak model is the heat flow from the two components. The heat soak model for the combustor is illustrated in figure 24 and figure 25 shows how it was implemented in Dymola. Thermal radiation from the combustor to the casing has previously been neglected due to the fact that film cooling occurs on the outside of the combustor. Heat transfer only occurs from convection between the fluid and the metal components.
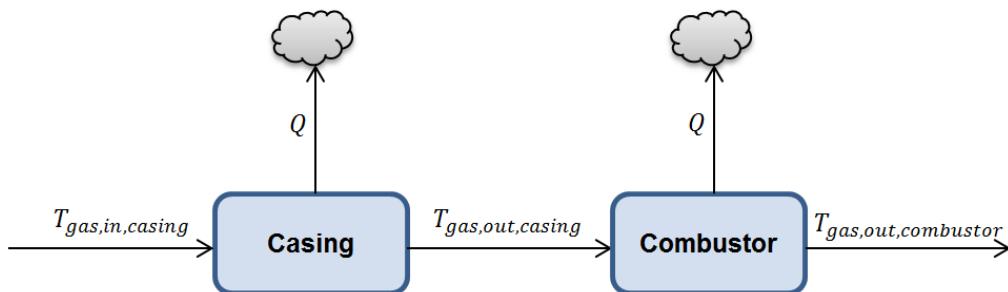

*Figure 24 – Illustration of the heat soak model of the combustor.*
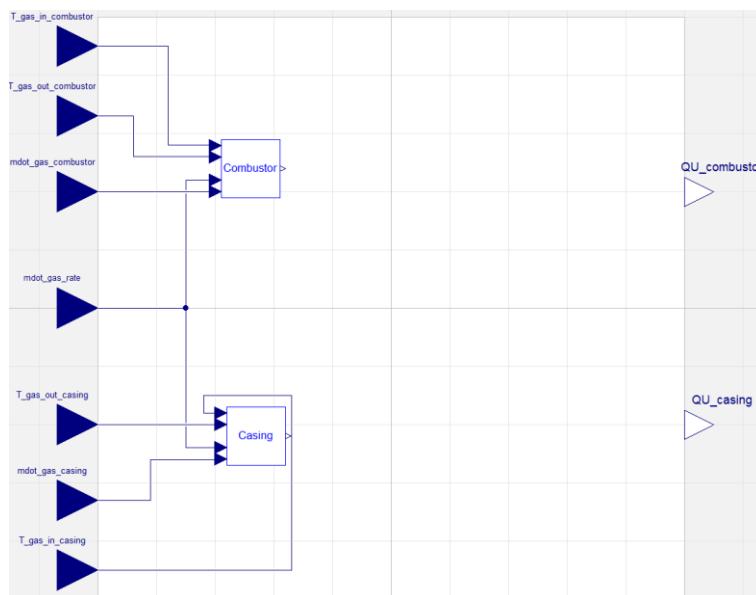
Figure 25 – Schematic picture of how the heat soak model in Dymola of the combustor is structured.

Implementation of heat soak model into combustor model
The heat soak model was implemented into the existing combustor model in Dymola illustrated in figure 26. The inlet temperature at the casing was set to the feed temperature of the combustor model. To calculate the outlet temperature of the casing the influences of heat soak needs to be added.

$$T_{gas,casing,out} = T_{gas,casing,in} - \frac{Q_{casing}}{\dot{m} \cdot c_p} \tag{79}$$

The outlet temperature from the combustor is set to drain temperature from the compressor.

A total value of the energy flow from casing and combustor is complied.

$$Q = Q_{casing} + Q_{combustor} \tag{80}$$

The total energy flow from the central casing and the combustor is implemented in the energy balance equation for the existing combustor model.

$$H_{air,inlet} + H_{fuel,inlet} - H_{gas,outlet} - Q_{rad} - Q = 0 \tag{81}$$

where H is the enthalpy and Q_{rad} heat dissipation loss.

The mass flow at a reference case is implemented as a parameter and needs to be adjusted to different operational conditions.
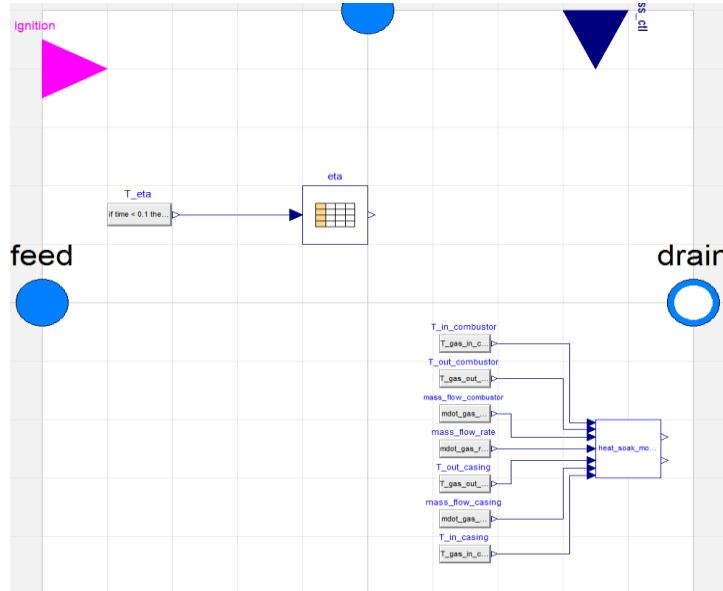

Figure 26 – Implementation of heat soak at combustor.

After heat soak was applied to the combustor model an analysis was made where influence of heat soak to the gas channel temperature was studied.

3.3.3 Turbine model

Heat soak at the turbine was applied to all three stages. The heat soak model was kept as uncomplicated as possible without venturing the accuracy of the model. The cooling effects are complicated especially when heat transfers at cooled objects such as blades, vanes and disks in the turbine. In this project the average temperature between the cooling flow and the main flow was assumed to affect cooled components in the gas channel. The first two stages of blades and vanes are cooled with air and the third stage is uncooled for the SGT-800.

Heat soak model for a stage

The heat soak model for a stage constitutes the basic equation. In fact, it has exactly the same appearance as the heat soak model for a stage at the compressor. It is illustrated in figure 27. One of the requests for this project was to generate a general heat soak model which would be easy to integrate into any component.

The surface area and thermal mass were obtained from a CAD program. The thermal mass and surface areas comprise blades and vanes for all three stages and the heat shield from the first two stages.

The specific heat was retrieved from a table of the metal components in the turbine.

The heat transfer coefficient from a reference case was computed with the help of the turbine aero department at SIT. The heat transfer coefficient was computed with a 2D thermal state program.

The heat transfer coefficient at a reference case for each stage in the turbine is defined as

$$Re = Re_C \frac{\rho \cdot u_\infty \cdot d_h}{\mu} \tag{82}$$

where Re_C is Reynolds correction factor and d_h is the hydraulic diameter.

$$Pr = \frac{c_p \cdot \mu}{k} \tag{83}$$

Nusselt number from the Dittus-Boelter correlation

$$Nu = 0,021 Re^{0,8} Pr^x \tag{84}$$

Nusselt number from derivation

$$Nu = \frac{HTC \cdot d_h}{k} \tag{85}$$

Combining equation 84 and 85 gives

$$HTC = \left(\frac{k}{d_h}\right) 0,021 Re^{0,8} Pr^x \tag{86}$$

The heat transfer coefficient depends on temperature and mass flow for a reference case. The same scaling as for the compressor is used.

$$HTC(t) = HTC_{ref} \cdot \left(\frac{\dot{m}(t)}{\dot{m}_{ref}}\right)^{0,8} \cdot \left(\frac{\dot{T}(t)}{\dot{T}_{ref}}\right)^{0,22} \tag{87}$$
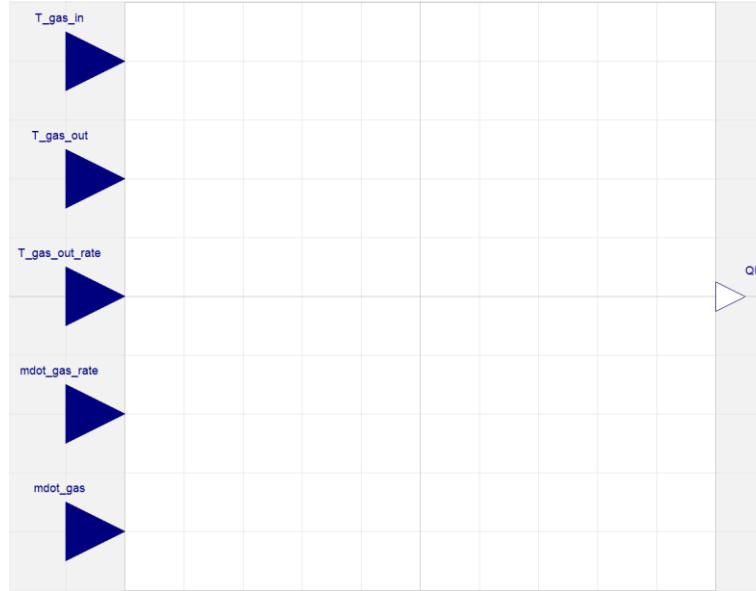

Figure 27 – Illustration of the basic heat soak model for the turbine.

Heat soak model
The heat soak model for the turbine consists of heat soak occurring at all three stages. The gas temperatures in and out of the turbine are known but not the temperature at each stage. An assumption was made that the temperature decreases across all stages in the turbine and it was set to the same value. The temperature at each stage is a combination of temperature of main flow and the temperature of cooling air. The temperature that enters the stage is exposed to heat soak from the previous stage which makes the model more accurate to a real gas turbine. The mass flow is increasing through the turbine due to the addition of cooling air at each stage. The combined energy flow from the three stages constitutes the output of the model. A schematic picture and an illustration in Dymola of the heat soak model of the turbine are presented in figures 28 and 29 respectively.
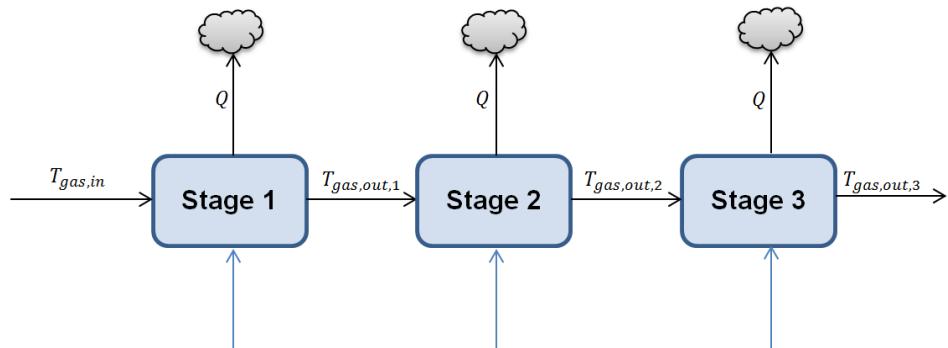

*Figure 28 – Illustration of the heat soak model of the combustor.*

31
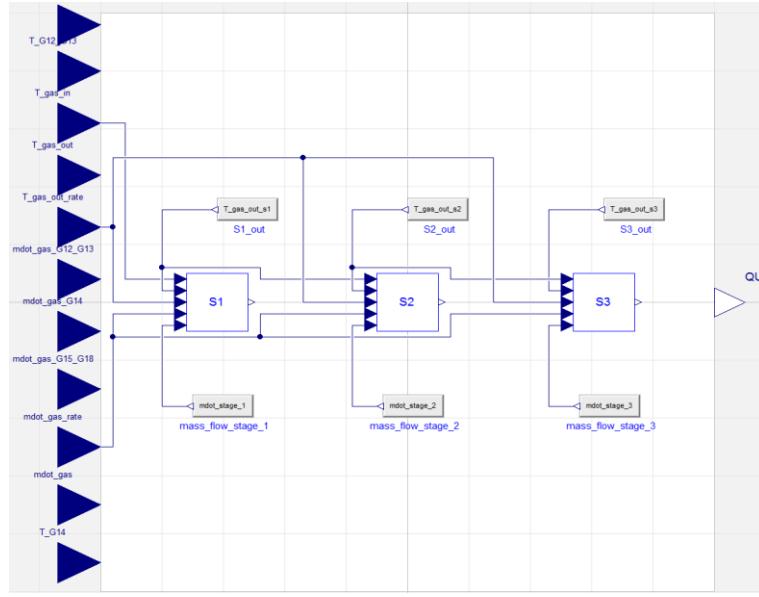
Figure 29 – Schematic picture of how the heat soak model in Dymola of the combustor is structured.

Implementation of heat soak model into turbine model

The implementation of the heat soak model into the existing turbine model is shown below in figure 30. The inlet temperature to the heat soak model was set to the feed temperature from the turbine model and the outlet temperature of the heat soak model was set to the drain temperature of the turbine. The injected mass flows and temperatures are heritage from values of extraction at the compressor. Parameters for scaling the heat transfer coefficient are implemented. Heat flow between main flows and metal components is implemented to the energy balance equation at the excising turbine.

$$H_{inlet} + \dot{m}_{power} \cdot \Delta h + H_{injection} - H_{outlet} - H_{windage\ loss} - Q = 0 \qquad (88)$$

Δh is the isentropic enthalpy difference after injection, $H_{injection}$ is the enthalpy from injections and $H_{windage\ loss}$ are the windage losses of the turbine.
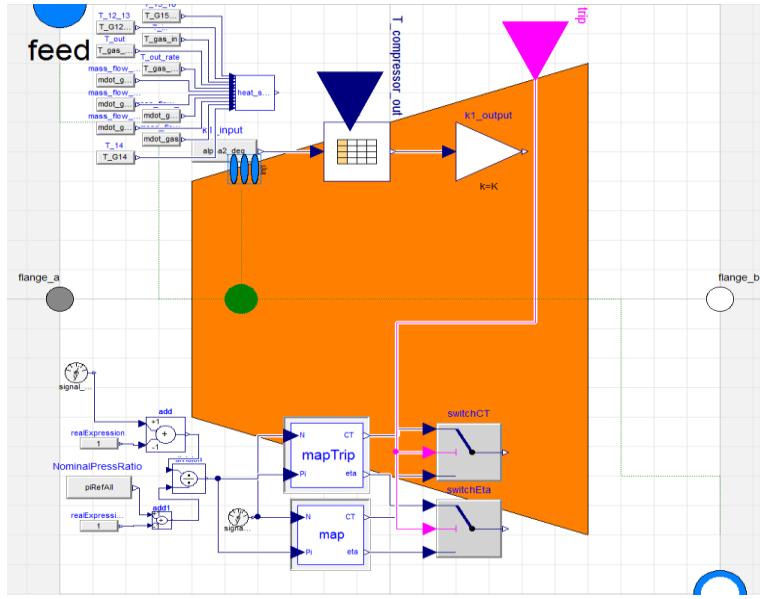
Figure 30 – Implementation of heat soak at combustor.

After heat soak was applied to the turbine model an analysis was made where influence of heat soak to gas channel temperature was studied.

3.4 Validation towards measured data

Measured data are compared to the SGT-800 model in Dymola with heat soak implemented to ensure the accuracy of the model.

STA-RMS and TeMas were used to find useful data at different operation conditions such as a start, a stop and a trip. To find good measured data without measurement disturbances was an arduous task. Data from different sites were evaluated to exclude errors and ensure validity. Most of the data used in this project are from prototype tests of the first SGT-800B model and from the test rig TRIFS3 located at SIT in Finspång, Sweden.

During a comparison of the heat soak model and the measured data several parameters must be adjusted according to operational condition and ambient condition in the heat soak model. Parameters such as barring speed, purge speed and ignition speed need to be defined. Time setting as time to synchronize also needs to be set to get the model to accord to measured data.

The heat soak model in Dymola was compared to several measured data configurations of different operational conditions and ambient conditions to define the difference. Tuning in parameters of the heat soak model and implementing inertia for probes decrease the difference and will be described in the following sections.

3.5 Tuning in heat soak model

To obtain a more accurate result the temperature difference in the gas channel is tuned in by adjusting parameters such as thermal mass and heat transfer coefficients in the heat soak model. An analysis was conducted to investigate the impact of changing heat transfer coefficients and thermal mass for the compressor, the combustor and the turbine, by analyzing gas channel temperatures. Heat transfer coefficients and thermal masses were change in the compressor for different rates. The thermal masses and heat

33

transfer coefficients were increased by 20 per cent, 100 per cent and 900 per cent in the compressor. The result is shown in the result chapter, figure 34.
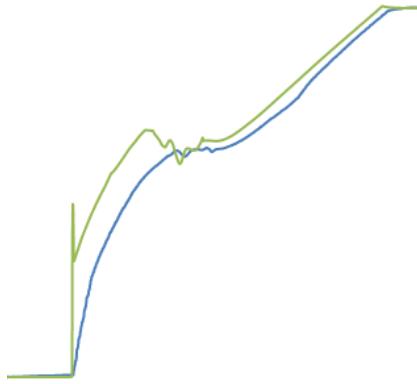
Figure 31 – Tuning heat transfer coefficient and thermal mass to manage the gas channel temperature to accord more towards measured data.

The change of outlet turbine temperature was studied when heat transfer coefficient and thermal mass were changed in the combustor and turbine. The thermal masses and heat transfer coefficients were increased by 20 per cent and 100 per cent respectively and can be further studied in figures 35 and 36 in the result chapter.

From studying the change of heat transfer coefficient and thermal masses optimal values were chosen to get the computed values to accord more towards measured data. The exhaust gas temperature for optimal values of thermal mass and heat transfer coefficient is illustrated in figure 31. The Impact of changing heat transfer coefficient and thermal mass is further presented in the result chapter.

3.6   Implement inertia for probe models

Inertia in probes needs to be taken into account in the dynamic gas turbine to correlate gas channel temperature between model and measured data. To emulate the inertia in the probe that occurs due to the encapsulation of the thermocouple of metal, a first order function was implemented to temperature measurement points in the gas channel. The first order function was implemented to measurement points at compressor and turbine outlets. Figure 32 shows the implementation of the probe inertia in the dynamic gas turbine model.
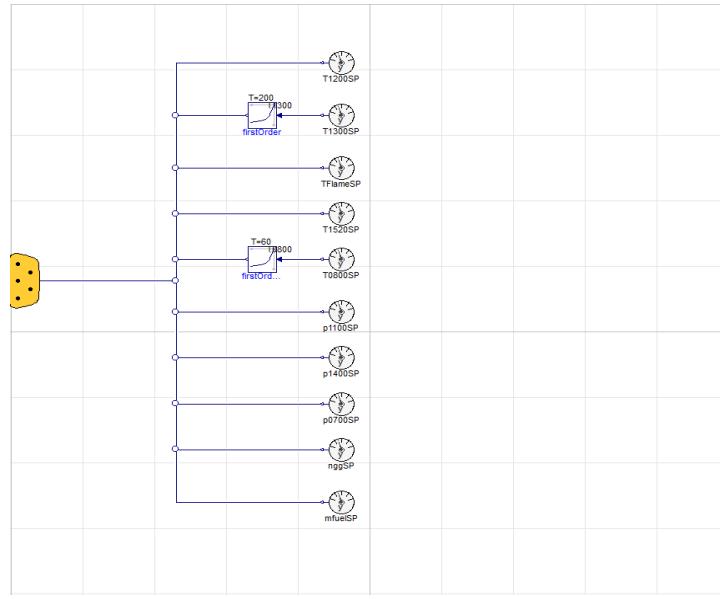
Figure 32 – Implementation of probe inertia to the dynamic gas turbine model in Dymola.
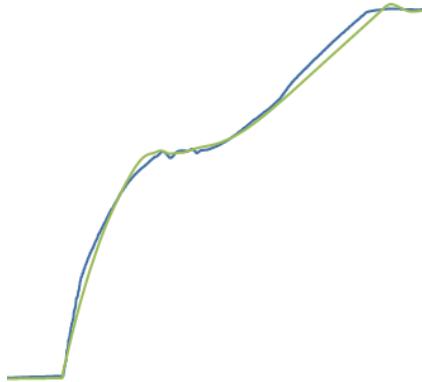
Figure 33 – Illustration of the difference of exhaust gas temperature implemented with heat soak and probe inertia in Dymola and measured exhaust gas temperature.

To regulate the amount of inertia the time constant T was changed to find the inertia in the dynamic model that mimics the real probe in a realistic way. It is illustrated in figure 33 above.

$$Y(s) = \frac{G}{T \cdot s + 1} \cdot U(s) \qquad (89)$$

3.7 Validation of model

A validation of the dynamic model in Dymola of SGT-800 was conducted towards data from different sites and during different ambient conditions. Gas and metal temperatures in the gas channel during different operating conditions as start, stop and trip were plotted in different charts. In these charts the transient behavior was analyzed. Several other parameters as mass flow, power output and rotational speed were evaluated to ensure the conformity to measured data. A wide spectra of tests have been evaluated to ensure that the heat soak model is applicable for a general SGT-800.

4 Results

This chapter presents a compilation of all results describing the dynamic behavior of the SGT-800 model implemented with heat soak. All charts have been normalized to make it possible to publish the report without compromising any vital information. More thorough information regarding the results and how they were obtained can be found in the methodology and discussion chapters.

4.1 Tuning in heat soak model

The heat soak model was tuned in towards measured data by changing heat transfer coefficient and thermal mass for the compressor, the combustor and the turbine parts. The influence of changing heat transfer coefficient and thermal mass on gas channel temperatures is studied in this section. Values of heat transfer coefficient and thermal mass were computed with an uncertainty that gives the possibility to alter these parameters towards measured data within a realistic level. The thermal mass operates as inertia in the heat soak model and the heat transfer coefficient affects the amount of heat that is possible to transfer per time unit.

4.1.1 Compressor model

Heat transfer coefficient and thermal mass were changed for all fifteen stages at the compressor. The chart defines the compressor outlet temperature as a function of time.

The Basemodel in the chart defines the gas turbine model in Dymola and the Heat soak defines the gas turbine implemented with heat soak with computed heat transfer coefficients and thermal masses. The other plots show the influence of changing heat transfer coefficient and thermal mass according by their name in the chart. Changing heat transfer coefficient and thermal mass in a reasonable level does not increase the influence of heat soak to a large extent. It is only when heat transfer coefficient and thermal mass are changed with high numbers that a difference can be seen, in this case a 900 per cent increase.
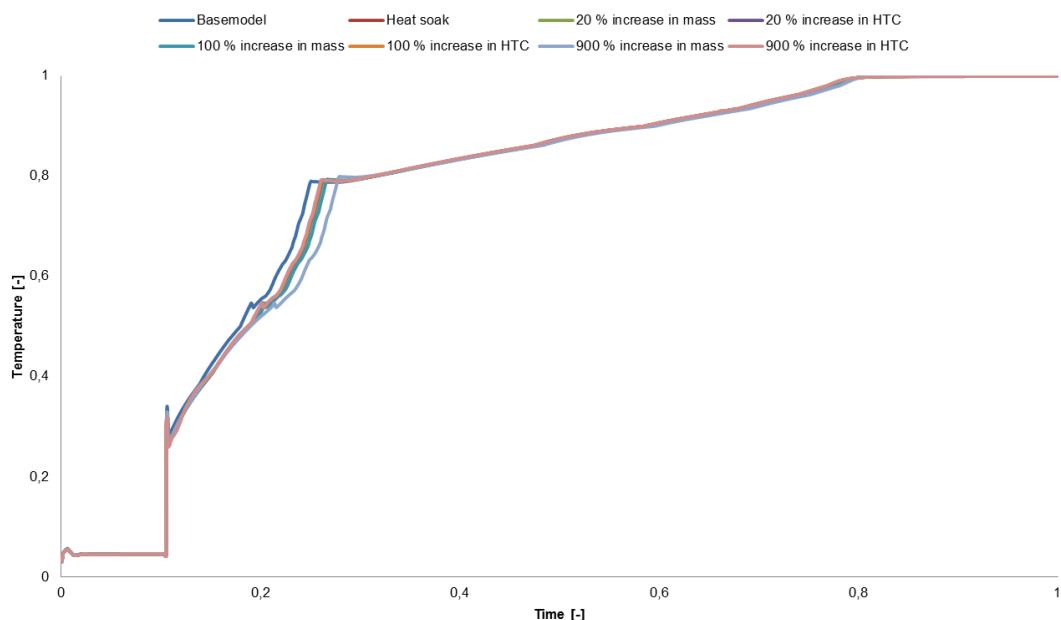
Figure 34 – Illustration of the impact of compressor outlet temperature by changing HTC and thermal mass.

4.1.2 Combustor model

The chart below describes the influence of changing heat transfer coefficient and thermal mass at the combustor on exhaust gas temperature. As in the previous chart a gas turbine model with and one without heat soak are plotted. To illustrate the influence of changing heat transfer coefficient and thermal mass, a 20 per cent and a 100 per cent increase are plotted. Increasing thermal mass and heat transfer coefficient to some extent decreases the ignition peak at a start operation. Adding thermal mass in the combustor has a minor impact on increasing inertia in the exhaust temperature. This is illustrated in figure 35.
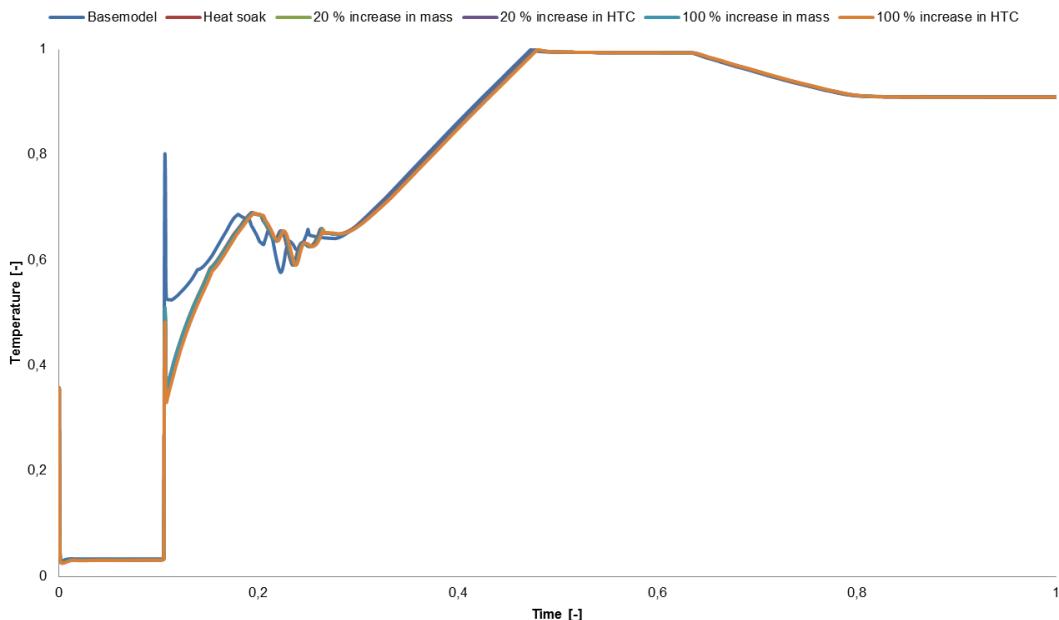
Figure 35 – Illustration of the impact on exhaust gas temperature by changing HTC and thermal mass.

4.1.3 Turbine model

The influence of changing heat transfer coefficient and thermal mass in the heat soak model for the turbine is illustrated in figure 36. Changing heat transfer coefficient and thermal mass in the turbine makes a larger impact in comparison to the compressor or combustor. The high temperature of the turbine combined with a relatively high amount of thermal mass make the impact of heat soak greater than the previously described components. The gas turbine model is plotted with and without heat soak. To describe the influence of changing heat transfer coefficient and thermal mass to the exhaust gas temperature a 20 per cent and a 100 per cent increase are illustrated in figure 36. The influence of changing heat transfer coefficient and thermal mass have a larger impact as expected but probe inertia needs to be implemented to simulate the measured temperature. Fast temperature change and peak heat flow can be reduced in the gas channel by alter thermal mass and heat transfer coefficient.
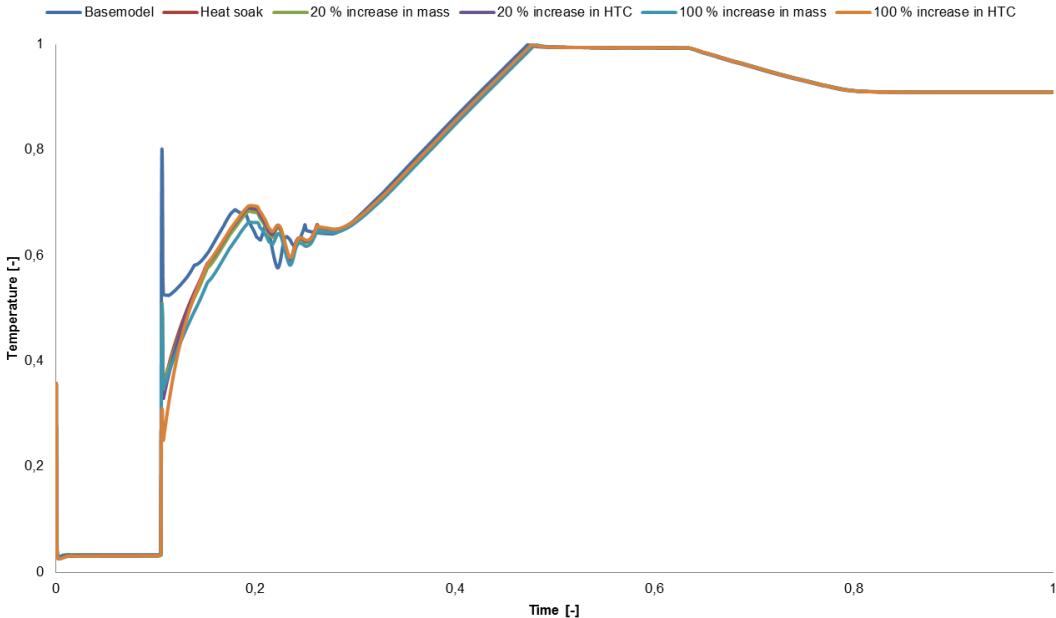
Figure 36 – Illustration of the impact on exhaust gas temperature by changing HTC and thermal mass.

4.2 Simulations of SGT-800 implemented with heat soak and probe inertia

In this section a compilation of all charts that were obtained during simulations of the SGT-800 with optimal tuned in values of heat soak and probe inertia is introduced. Several simulations with different operation conditions and ambient conditions were conducted to ensure the validity of the model implemented with heat soak and probe inertia.

4.2.1 Helsingborg test conducted 2010-04-27

Measured data from several tests performed during the prototype testing of the first SGT-800B were used in this project. Detailed documentation and low disturbances during transient operations as start, stop and trip make data from the Helsingborg test reliable.

Start operation

Figure 37 describes the exhaust gas temperature as a function of time during a start. Measured data are compared to different configurations of the dynamic gas turbine model in Dymola. The configurations are first the existing gas turbine model, second the gas turbine model implemented with heat soak and third the gas turbine implemented with heat soak and probe inertia. The third configuration is the one that was develop during this project and it represents the final result. The objective of this project was to implement heat soak and probe inertia to the existing gas turbine model and mimic as closely as possible the dynamic behavior of measured data during transients. The results from tuning in optimal values of parameters in the heat soak model resulted in an increase of the heat transfer coefficient by 10 per cent in the combustor, a 10 per cent increase of heat transfer coefficient at the turbine and increasing the thermal mass by 50 per cent in the turbine. Parameters in the compressor were not changed due to the small impact of changing parameters in the compressor.
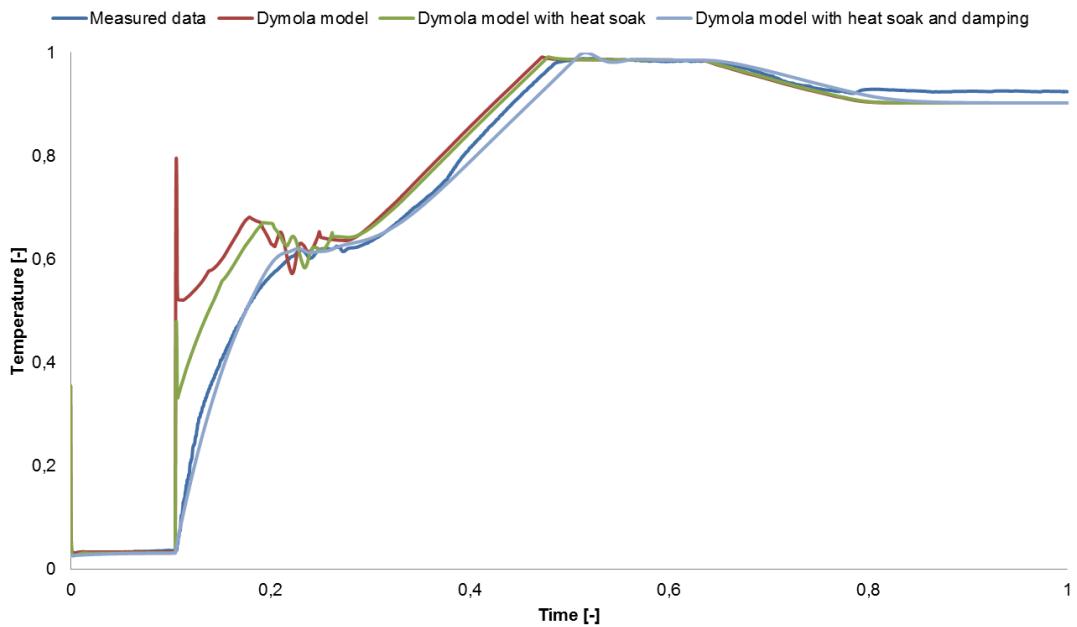
Figure 37 – Exhaust gas temperatures.

Figure 38 illustrates the compressor outlet temperature as a function of time during a start. Measured data are compared to the gas turbine model in Dymola implemented with heat soak and probe inertia. The Dymola model with heat soak and probe inertia corresponds well to measured data. Thus the model reacts too fast due to the lack of inertia in the model. In figure 38, the Dymola model, Dymola model with heat soak and Dymola model with heat soak and probe inertia are descibed. The effect of heat soak and probe inertia on the compressor outlet temperature are illustrated in figure 38. Flash back probes were included to describe how fast they react in comparison to probes located at the compressor outlet.
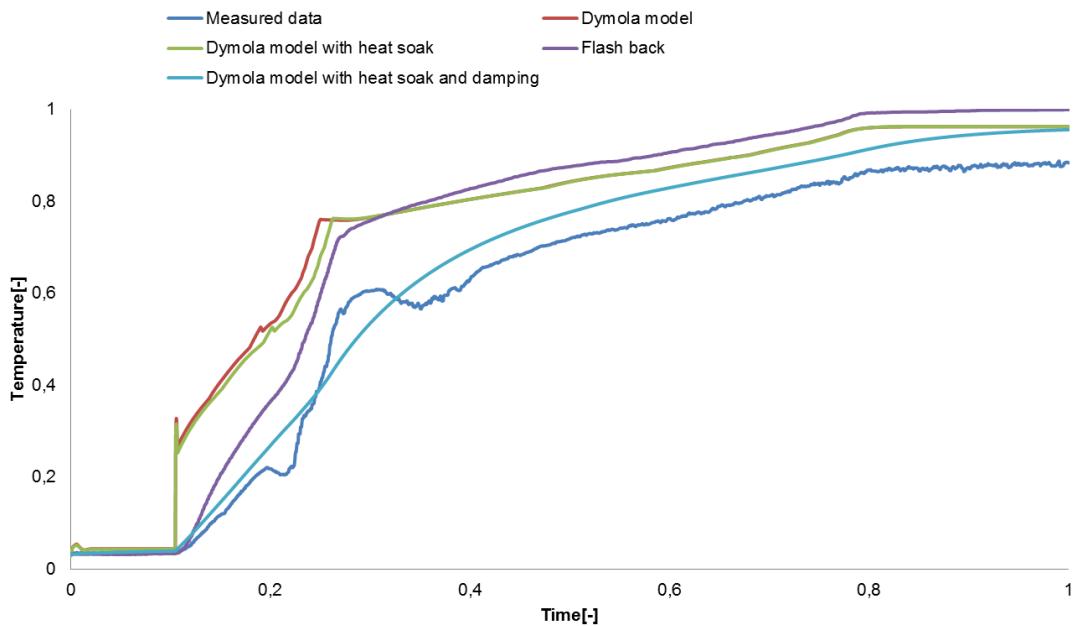
Figure 38 – Compressor outlet temperatures.

Metal temperatures during a start for each stage at the turbine are illustrated as a function of time in figure 39. The figure shows how fast metal components react at start operations. Figure 39 also provides an illustration of the temperature level in the turbine during a start but this can be misleading due to simplifications in the cooling of metal parts. In the gas turbine model in Dymola cooled air is added only to the inlet for each stage which gives a more correct gas channel temperature but not necessarily the right metal temperature.
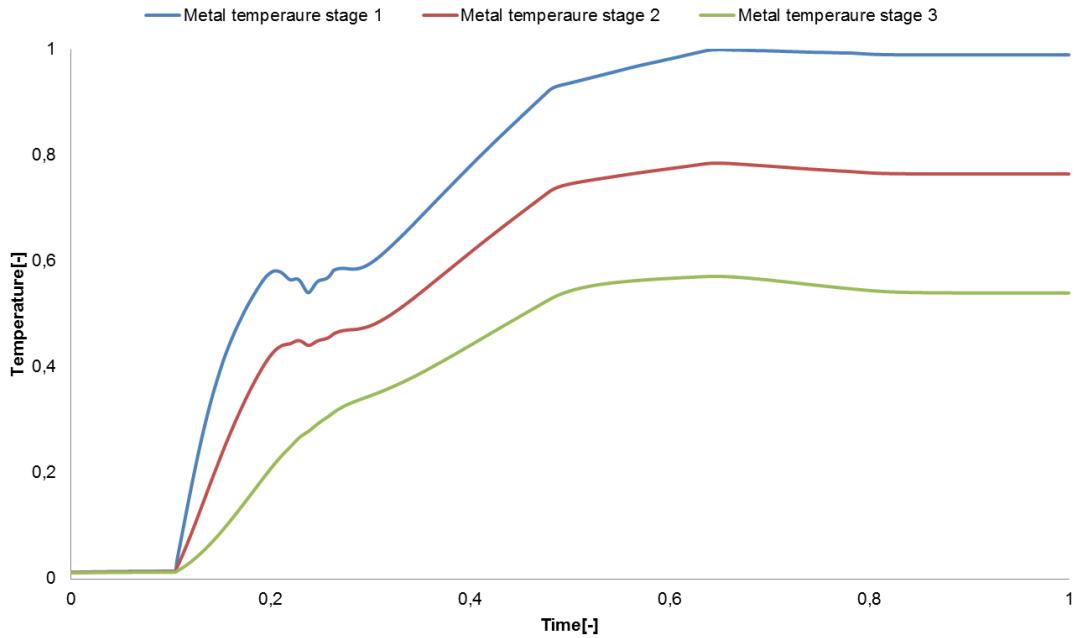
Figure 39 – Metal temperatures at the turbine.

Figures 40, 41 and 42 illustrate the influence between metal temperature and gas channel temperature during a start operation. The temperature difference between the gas channel and the metal component for each stage are illustrated. The inertia in metal components describes how fast the metal temperature reacts when gas channel temperature changes.

Figure 40, 41 and 42 describes temperatures in the first, second and third stage. Due to higher mass with higher stage number inertia is increased. It is illustrated in the following three charts.
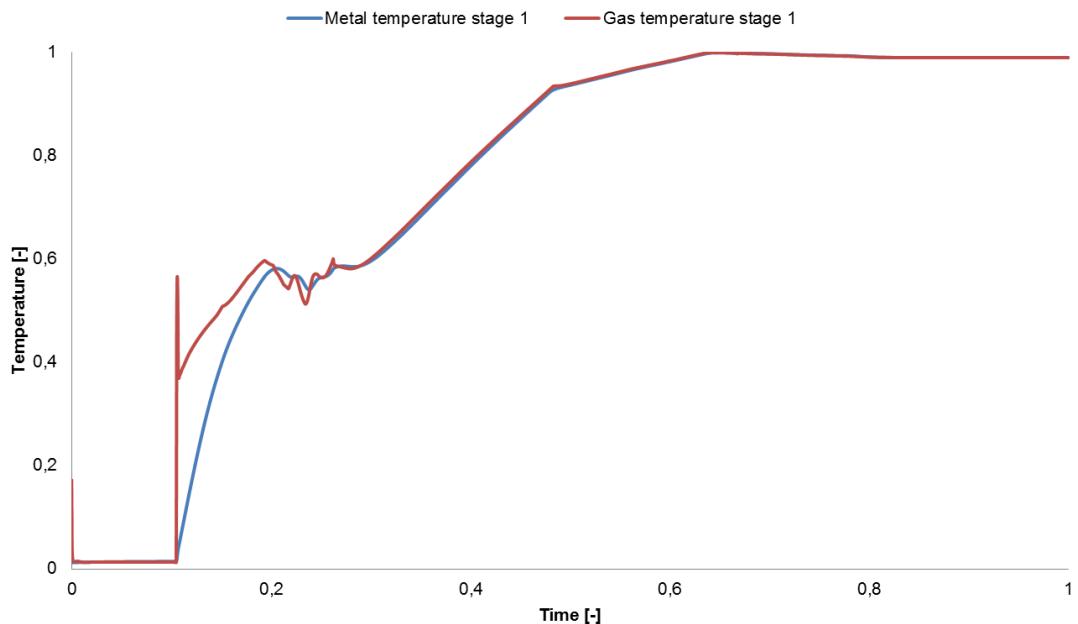
Figure 40 – Metal and gas temperatures at the first turbine stage.
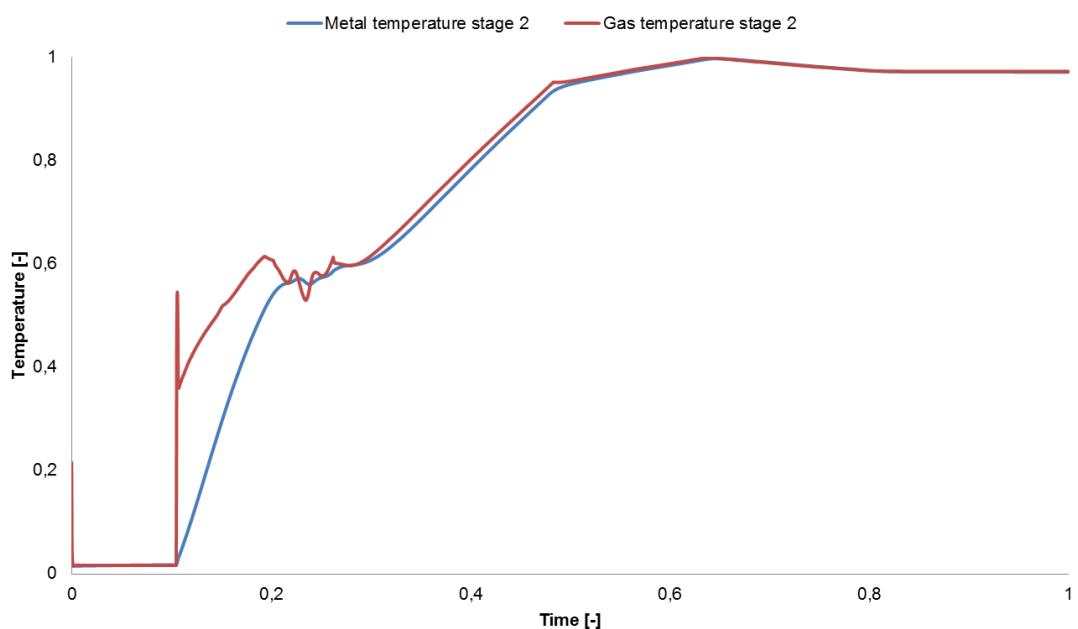
Figure 41 – Metal and gas temperatures at the second turbine stage.
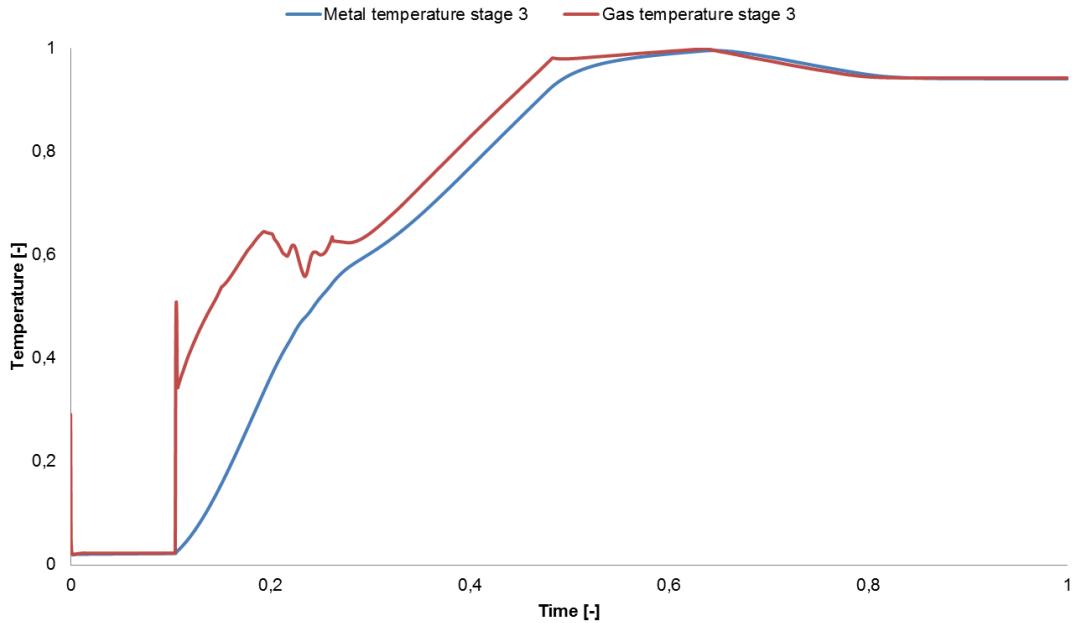
Figure 42 – Metal and gas temperatures at the third turbine stage.

Metal temperatures measured by thermo crystals at casing, first stage, second stage and third stage at the turbine are compiled in figure 43. A compilation between measured metal temperatures and computed values from the Dymola model is not well suited due to several simplifications which have been implemented in the dynamic gas turbine model in Dymola. In the gas turbine model metal temperature for each stage is assumed to be the same for casing, blade, vane and heat shield. The measured casing temperature constitutes an own measured point. Measured temperature for metal components are included to illustrate the effect of cooling.
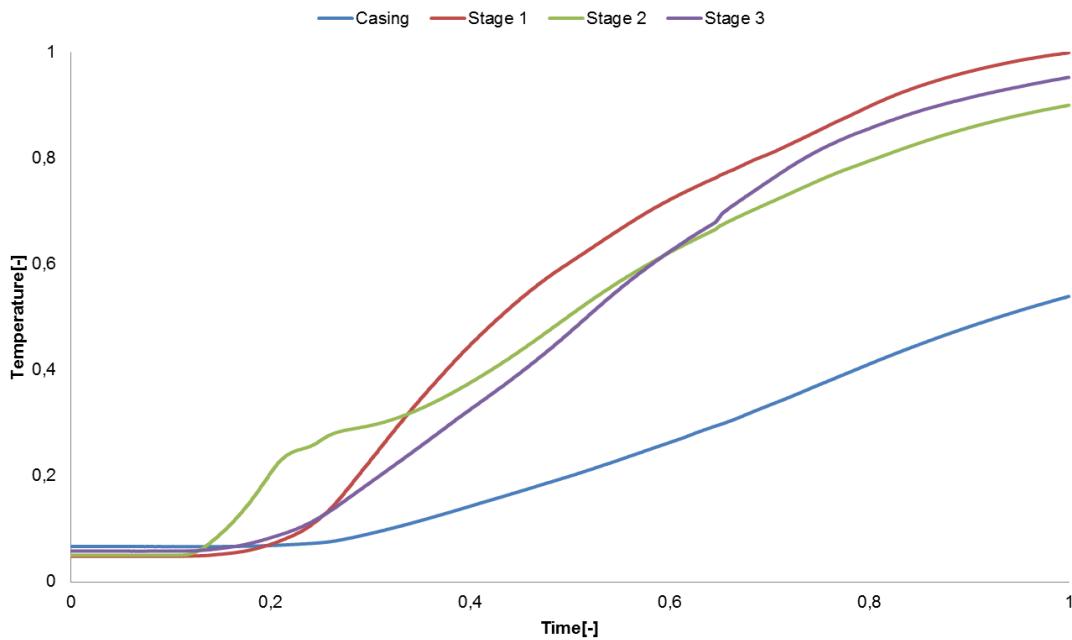
Figure 43 – Measured temperatures at turbine.

Gas channel temperatures of the dynamic gas turbine model are affected by implementing inertia from probes into the compressor outlet temperature and the exhaust gas temperature. The compressor outlet control temperature and the exhaust gas control temperature that regulates the gas turbine are affected by probe inertia. The gas channel temperatures get a higher temperature than the preferred and oscillate towards the set point temperature. Due to the value of the time constant in the transfer function the amount of oscillation can be controlled. The exhaust gas temperate has a large oscillation in comparison to the compressor outlet temperature. It is illustrated in figure 44.
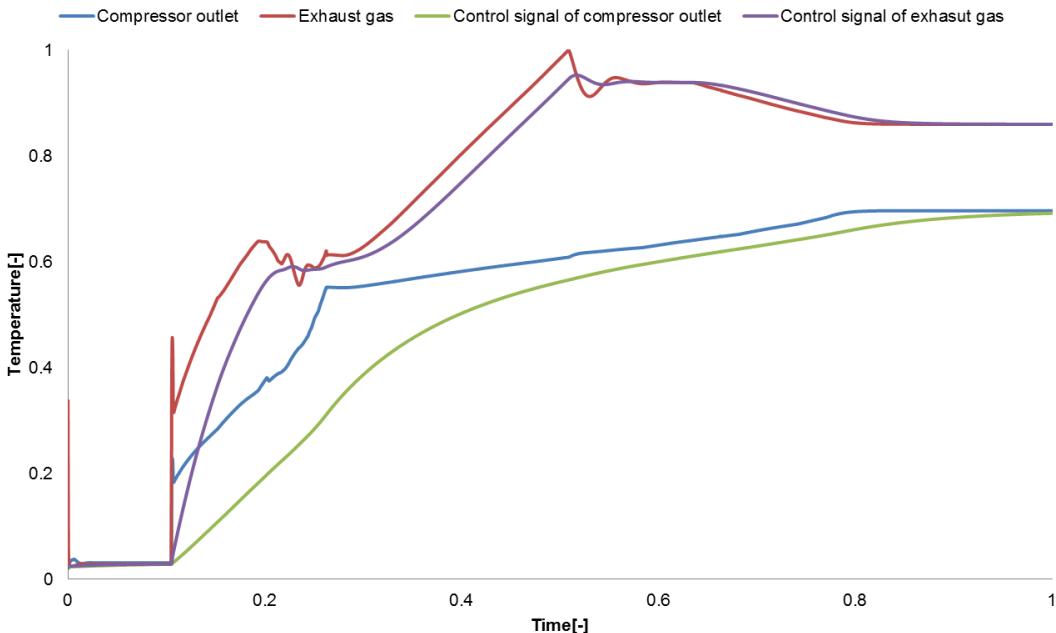
Figure 44 – Influence of inertia in probes.

Stop operation

Figure 45 describes the exhaust gas temperature as a function of time during a stop. Measured data are compared to different configurations of the dynamic gas turbine model in Dymola. As the start operation the included models are the gas turbine model, the gas turbine model implemented with heat soak, the gas turbine implemented with heat soak and probe inertia and measured data. The objective was to implement heat soak and probe inertia to the existing gas turbine model and mimic as close as possible the dynamic behavior of measured data during transients.

A large difference occurs between the measured exhaust gas temperature and the computed exhaust gas temperature from the gas turbine model in Dymola implemented with both heat soak and probe inertia. The gas turbine model implemented with heat soak and probe inertia has a slower reaction than the gas turbine model without heat soak and probe inertia but it is sensational faster than the measured temperature. This will be further discussed in the following chapter.

43
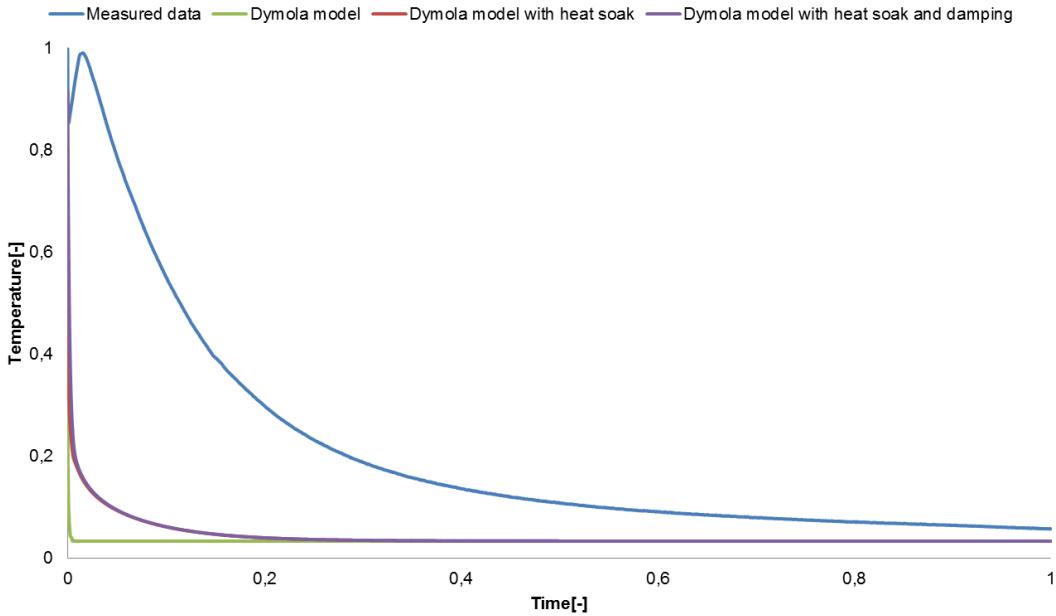
Figure 45 – Exhaust gas temperatures.

Figure 46 illustrates the compressor outlet temperature as a function of time during a stop operation. Measured data are compared to the gas turbine model in Dymola implemented with heat soak and probe inertia. As the exhaust gas temperature previously described the Dymola models reacts to fast compare to measured data. In figure 46 are models described as the Dymola model, Dymola model with heat soak and Dymola model with heat soak and probe inertia. The chart makes it possible to easily describe the effect of heat soak and probe inertia at the compressor outlet temperature.
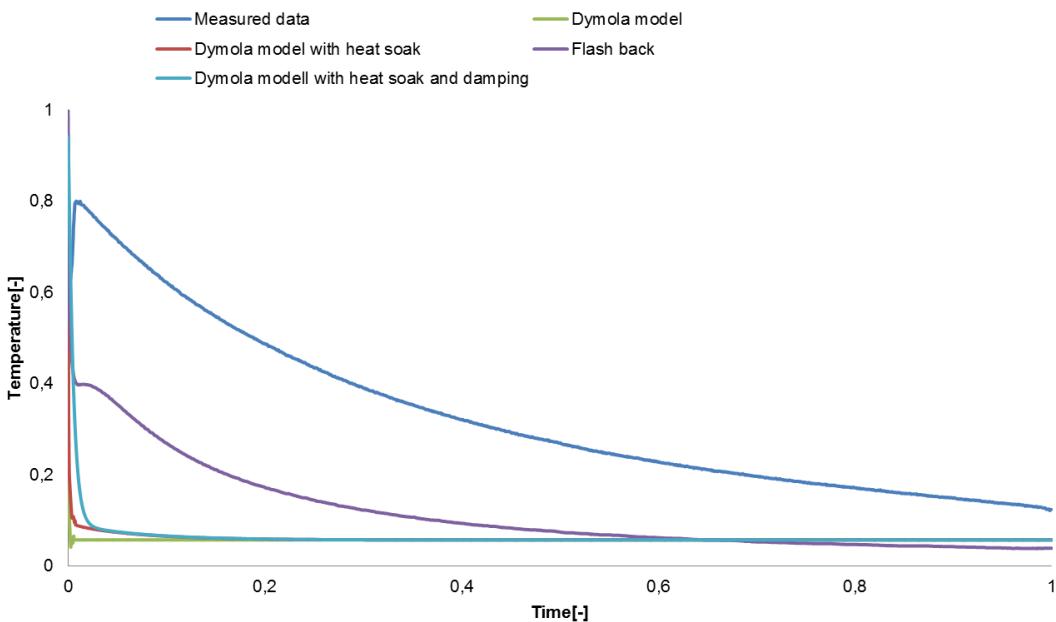
Figure 46 – Compressor outlet temperatures.

Mass flow in the compressor as a function of time during a stop operation is illustrated in figure 47. The mass flow at the compressor has been illustrated due to difference in gas channel temperatures between computed values from the gas turbine model in Dymola and measured data during stop operations. The gas turbine model crashes when the mass flow decrease under a certain level. Due to the gas turbine models instability during low compressor mass flows it is difficult to accord towards measure data. The measured data presented in the figure are not correct as well. The difference in mass flow at the compressor is further discussed in the following chapter.
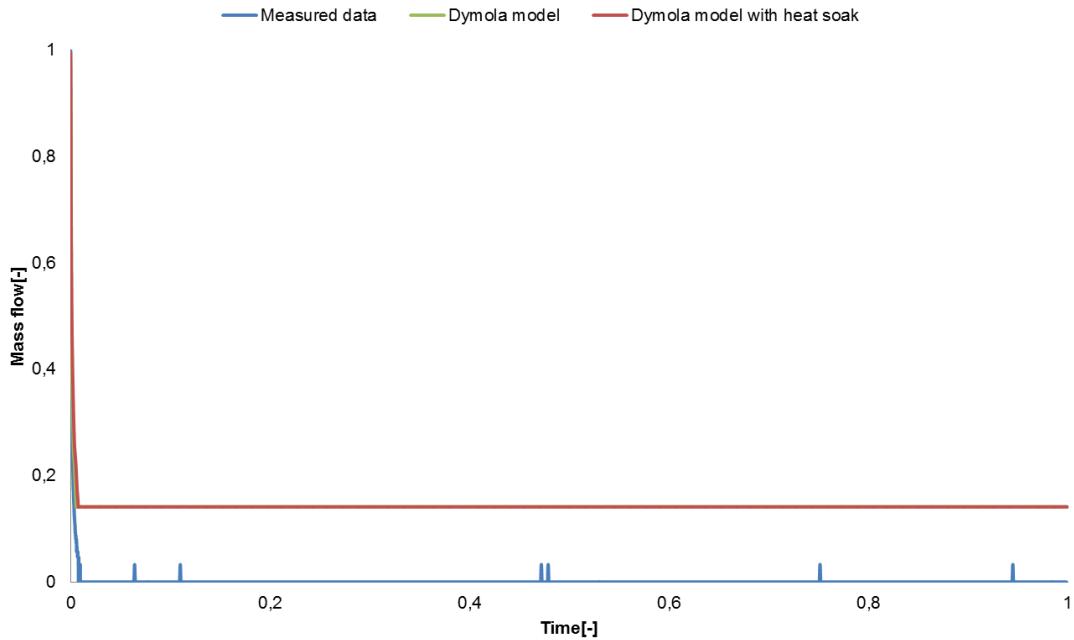
Figure 47 – Difference in mass flow between computed and measured data during a stop operation.

Metal temperatures for each stage in the turbine as a function of time during a stop operation are illustrated in figure 48. The purpose of the chart is to illustrate how fast metal components react at a stop operation. The stop operation is going on for a longer period than a start operation. The stop operation has a time span of approximately 11 hours in comparison to a start operation which is conducted during about 30 minutes.
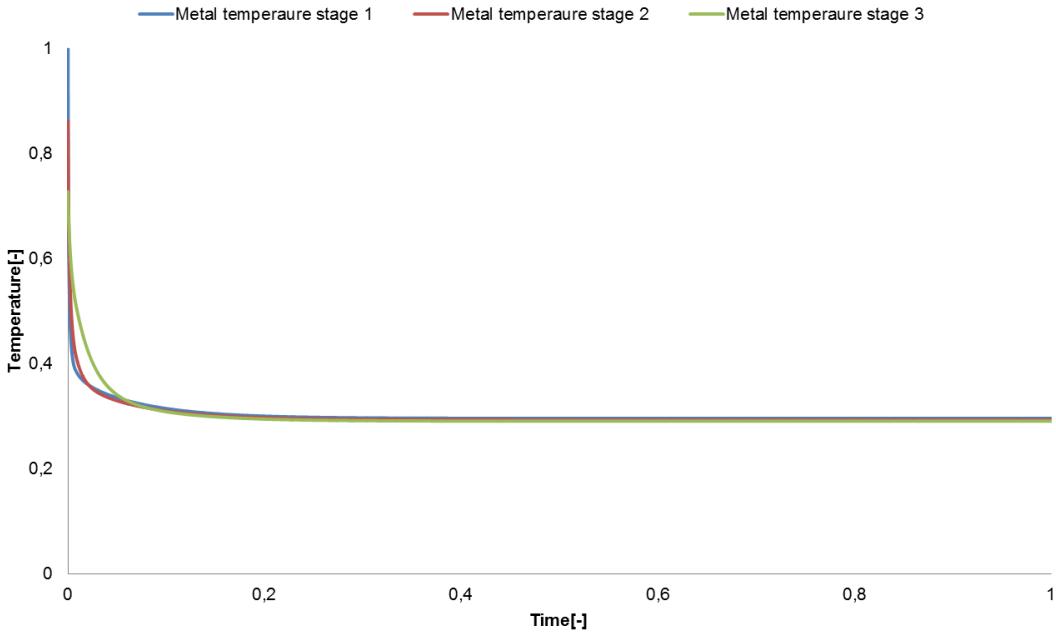
Figure 48 – Metal temperatures.

Figure 49, 50 and 51 illustrate the influence between metal temperatures and gas channel temperatures during a stop operation. A smaller time span has been used in the figures to get a clearer depiction of the change in gas channel temperature and metal temperature. Gas channel temperatures and metal temperatures are shown for each stage. The inertia in metal components describes by how fast the metal component reacts to temperature change in gas channel temperatures.

Figure 49, 50 and 51 describes temperatures in the first, the second and the third stage. Due to higher mass with higher stage number the inertia is increased. It is illustrated in the three following charts.
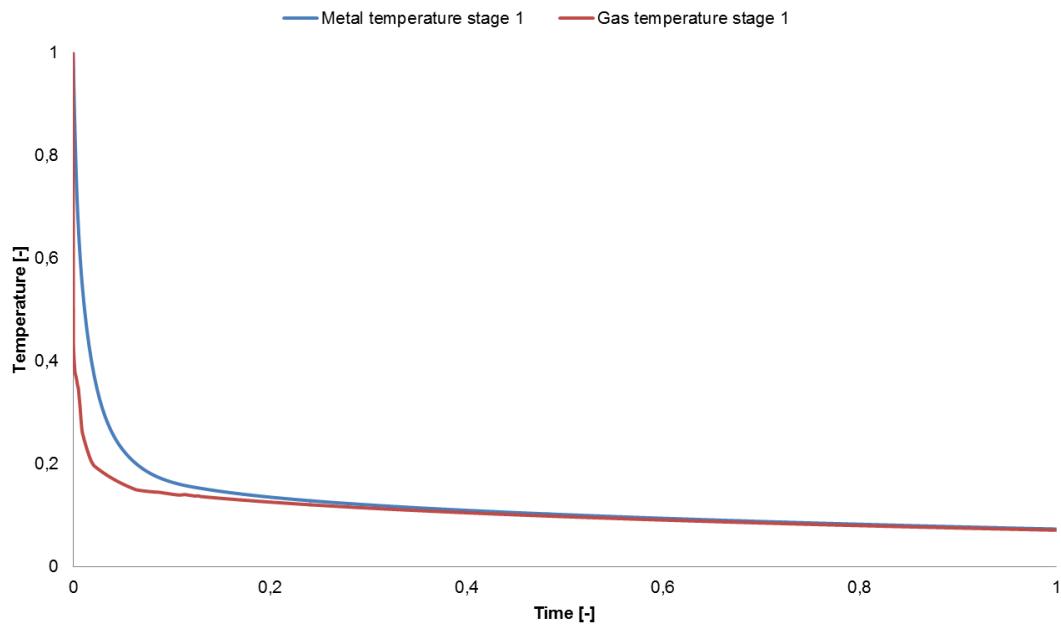
*Figure 49 – Metal and gas temperatures at the first turbine stage.*
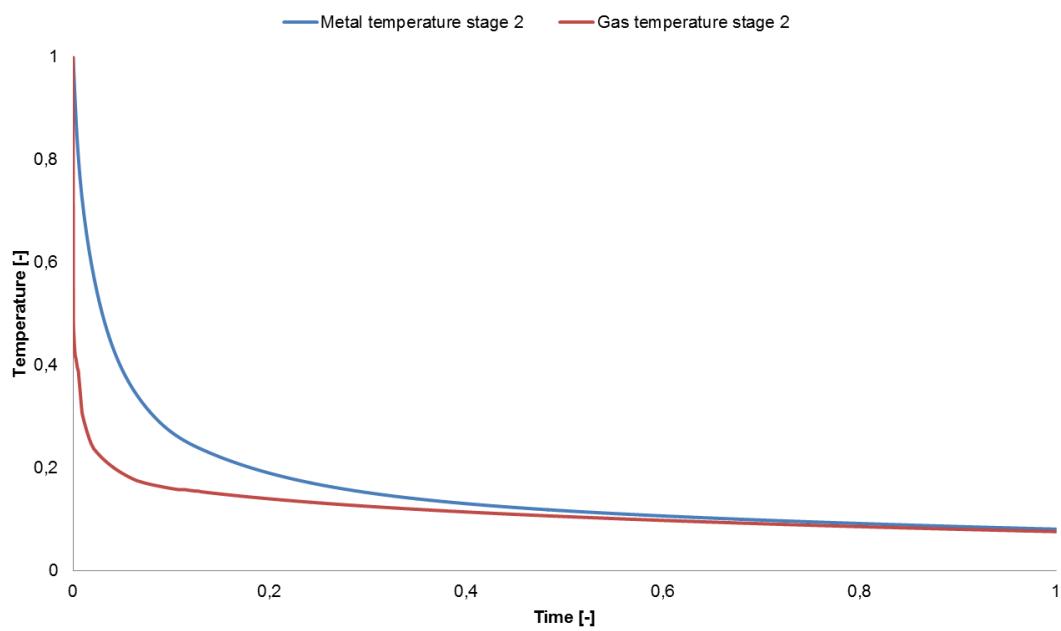
Figure 50 – Metal and gas temperatures at the second turbine stage.

47
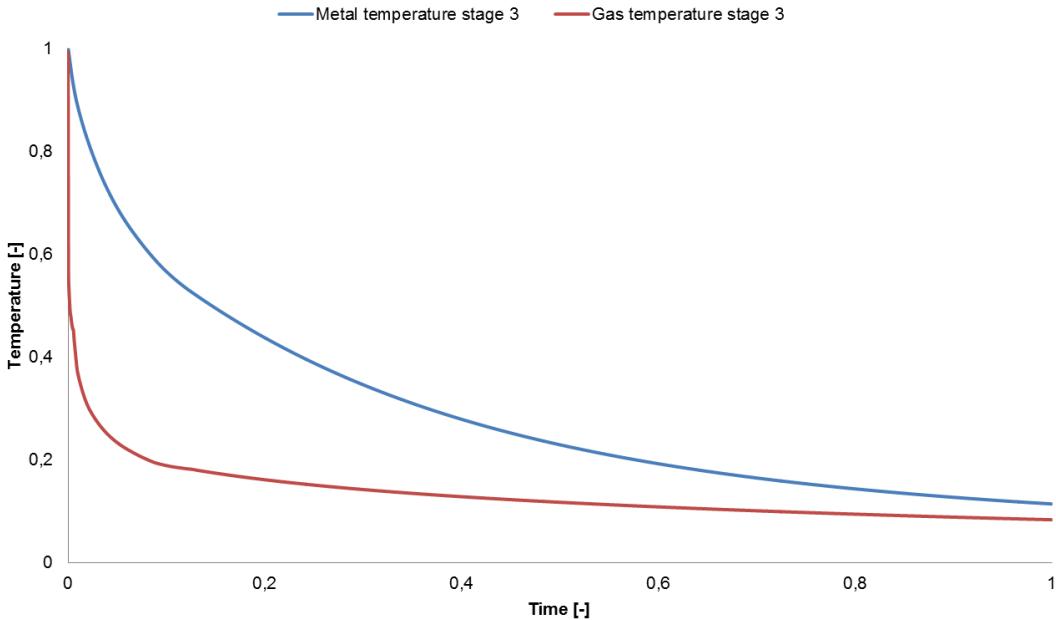
Figure 51 – Metal and gas temperatures at the third turbine stage.

Measured metal temperatures at casing, first stage, second stage and third stage at the turbine are compiled in figure 52. Due to simplifications made in the dynamic gas turbine model regard cooling flows a compilation between measured temperatures and computed temperatures are not well suited. A comparison of how fast measured data change to computed data from Dymoal is legitimate. Figure 52 below illustrates a large inertia in measured data in comparison to the computed values from Dymoal. The difference is further discussed in the following chapter.
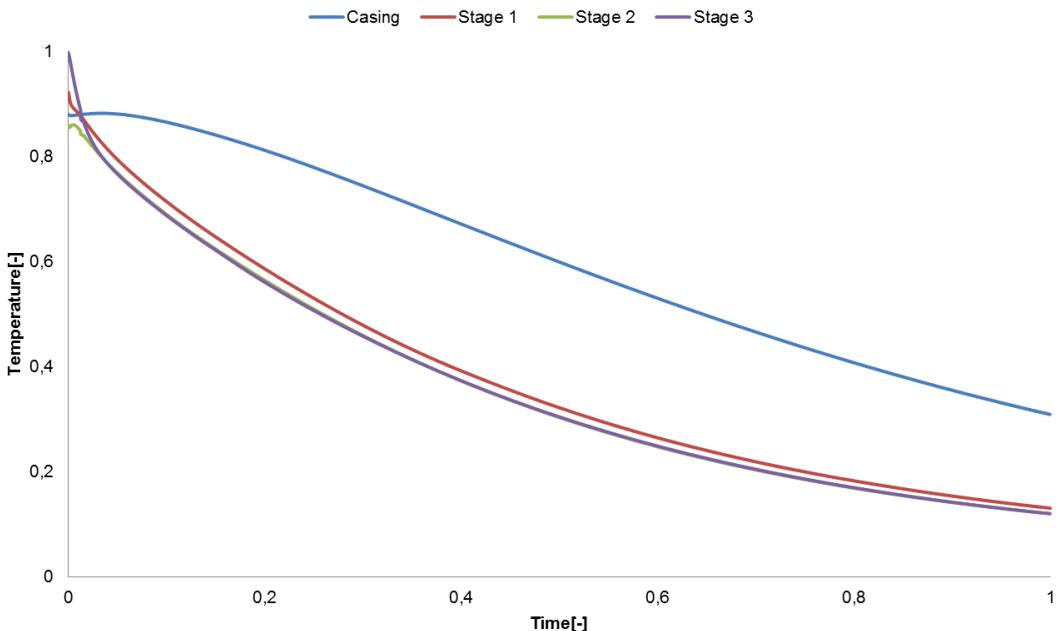

Figure 52 – Measured temperatures at the turbine.

Gas channel temperatures of the dynamic gas turbine model are affected by implementing inertia from probes into the compressor outlet temperature and the exhaust gas temperature. The gas channel temperatures get a higher temperature than the preferred and oscillate towards the set point temperature. Due to the value of the time constant in the transfer function the amount of oscillation can be controlled. During a stop operation the effect of oscillation for gas channel temperatures are small and are illustrated in figure 53.
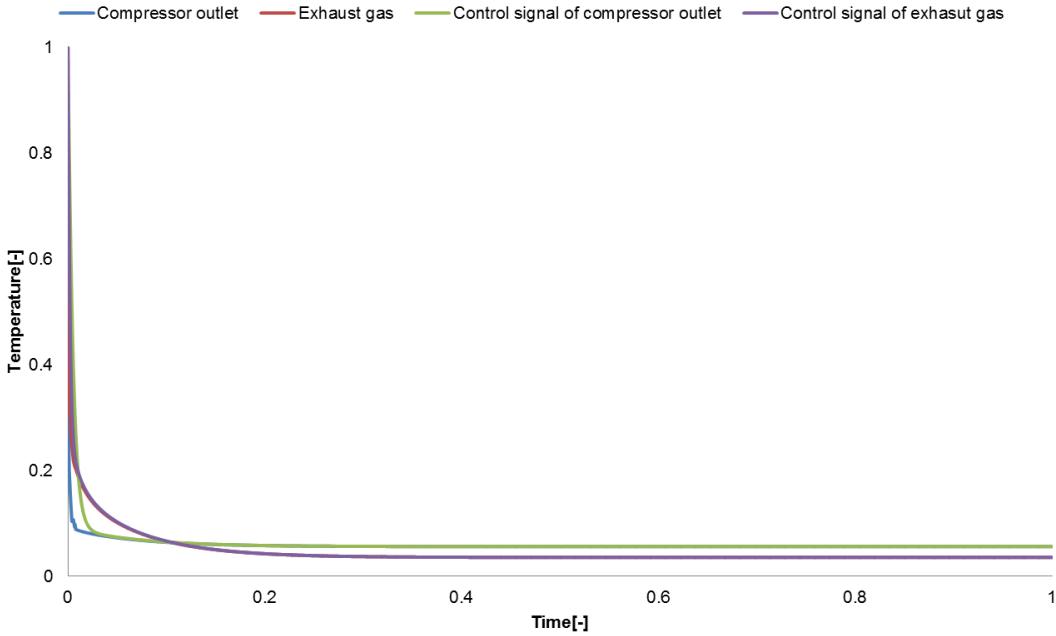

Figure 53 – Influence of inertia in probes.

Figure 54 illustrates both a start and stop operation during a time period. The purpose of the chart is to show how metal temperatures and gas channel temperatures compose to each other. Inertia in the different stages and at different operation conditions are easily to compared. It is illustrated in figure 54 that stage three possesses the highest inertia due to its large mass.
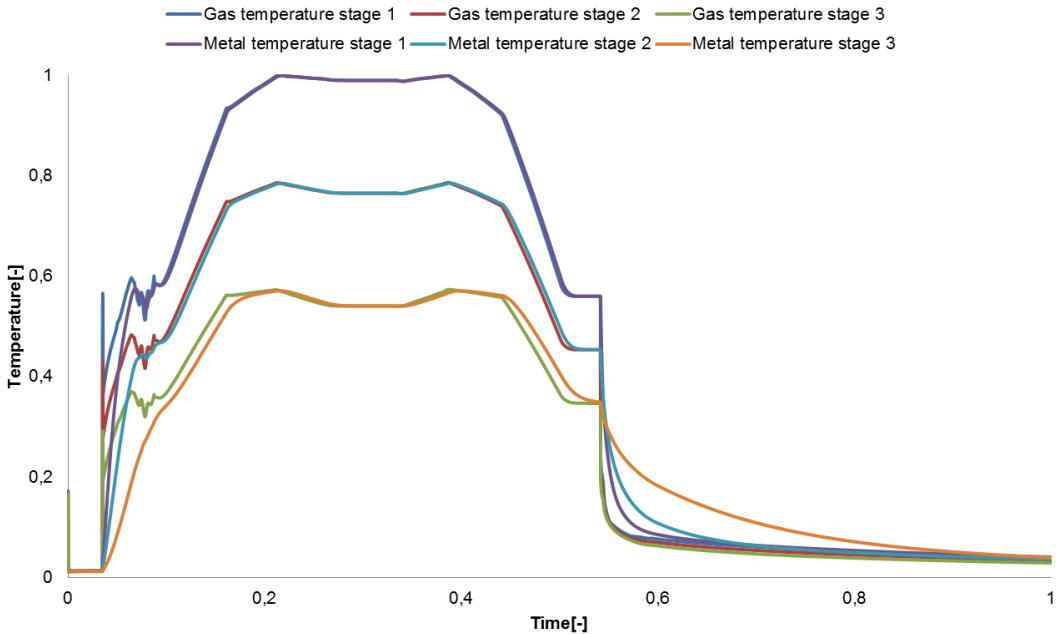
Figure 54 – Metal and gas temperatures at all stages in the turbine including both a start-up and shut-down operation.

4.2.2 Helsingborg test conducted 2010-05-20

This test was conducted in Helsingborg to evaluate an emergency shut down, a trip. The test was executed on the first SGT-800 model in Helsingborg.

Trip

During a trip the fuel of the gas turbine is instantly cut. In comparison a normal shut-down consist of a sequence of unloading operations followed by a fire shut down. Evaluation of how metal and gas channel temperatures interact during a trip are studied.

Figure 55 describes the exhaust gas temperature as a function of time during a trip. Measured data are compared to different configurations of the dynamic gas turbine model in Dymola. As for the start operation the included models are the gas turbine model, the gas turbine model implemented with heat soak, the gas turbine implemented with heat soak and probe inertia and measured data.

As a normal shut-down a large difference occurs between the measured exhaust gas temperature and the computed exhaust gas temperature from the gas turbine model in Dymola implemented with both heat soak and probe inertia. The gas turbine model implemented with heat soak and probe inertia is sensationally faster than the measured temperature. This will be further discussed in the following chapter.

50
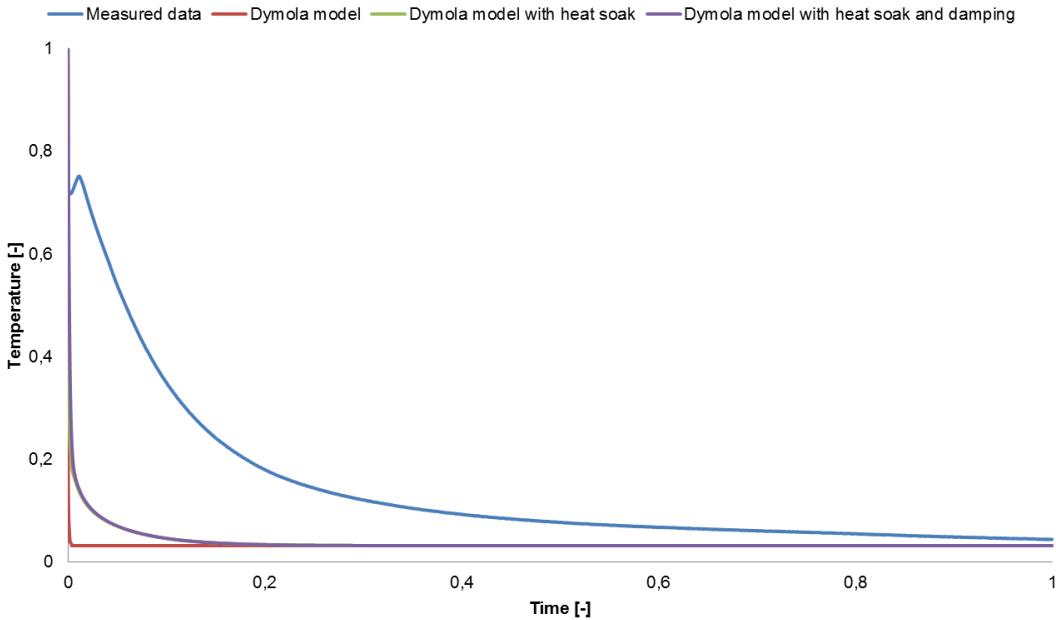
Figure 55 – Exhaust gas temperatures during a trip.

Figure 56 illustrates the compressor outlet temperature as a function of time during a trip. Measured data are compared to the gas turbine model in Dymola implemented with heat soak and probe inertia. The illustrated temperatures during a trip are essentially the same as a normal shut down. The Dymola models reacts too fast compared to measured data. In figure 56 models as the Dymola model are described, the Dymola model with heat soak and the Dymola model with heat soak and probe inertia. The chart makes it possible to easily describe the effect of heat soak and probe inertia at the compressor outlet temperature. Flash back probes react slower than Dymola models.
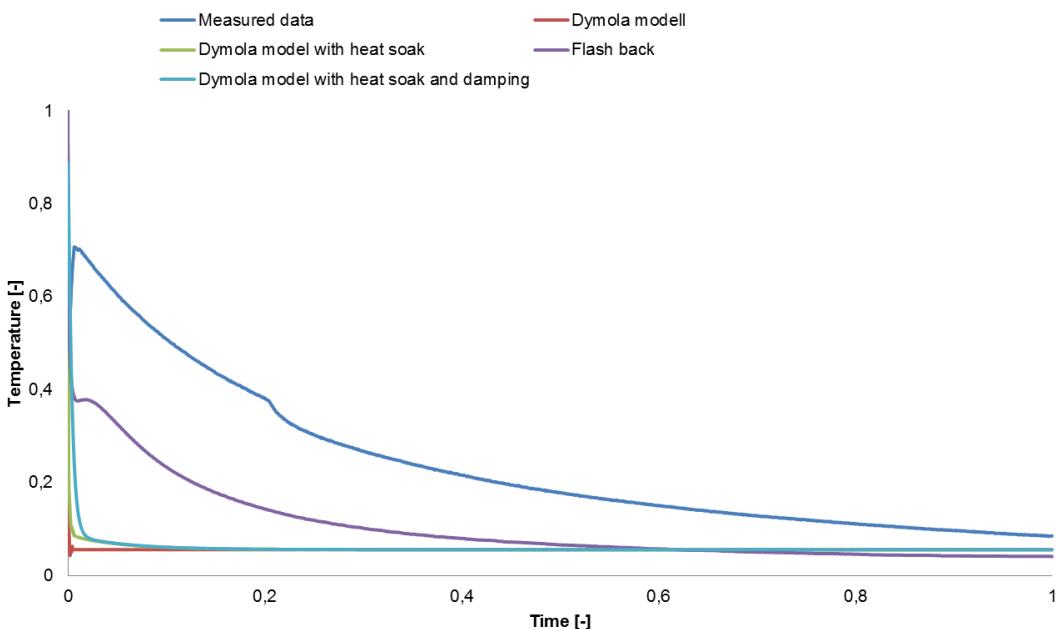

Figure 56 – Compressor outlet temperatures during a trip.

51

4.2.3 TRIFS test conducted 2016-04-28

This test was conducted at Siemens Industrial Turbomachinery's test facility in Finspång, Sweden. The test was used to tune in probe inertia to the compressor outlet temperature due to the tests low disorders.

Start

Evaluation of exhaust gas temperature and compressor outlet temperature for a start operation until load was applied. For the exhaust gas temperature its agreement to measured data was studied. The compressor outlet temperature was tuned in towards measured data due to the low disorder in this measurement. A good agreement of computed values and measured data are fulfilled and illustrated by the two charts below.
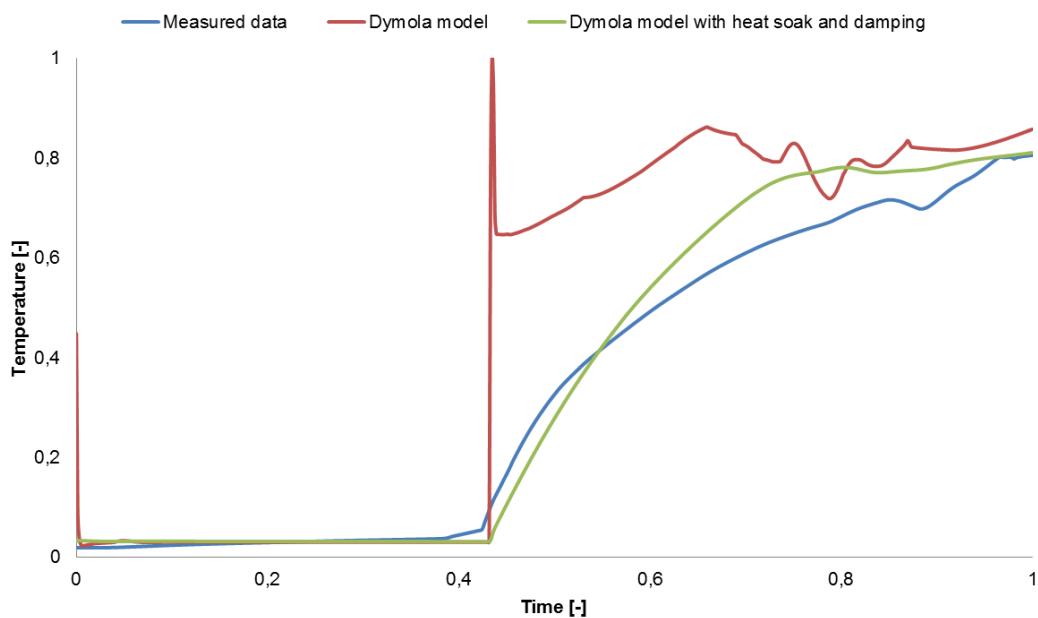

*Figure 57 – Exhaust gas temperatures.*
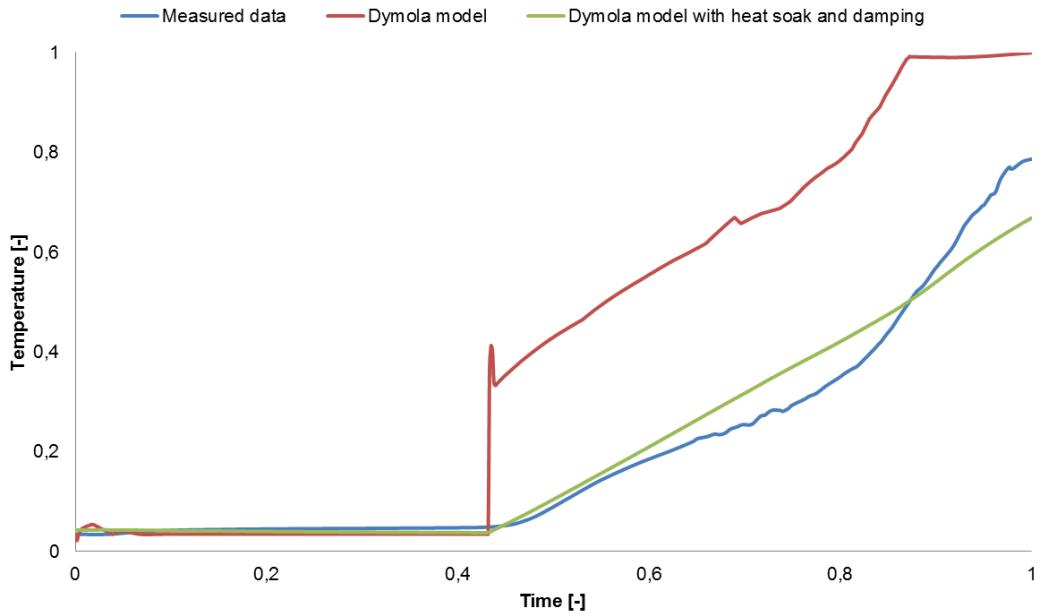
Figure 58 – Compressor outlet temperatures.

4.2.4 Helsingborg test conducted 2010-05-25

To ensure agreement of gas channel temperature implemented with heat soak and probe inertia to measured temperature, several different test were evaluated. Two tests from Helsingborg conducted on 2010-04-30 and on 2010-05-25 are demonstrated to assure agreement during different operational conditions and ambient conditions. Both charts have a good agreement between the gas turbine model implemented with heat soak and probe inertia and measured data illustrated in the charts.

Start
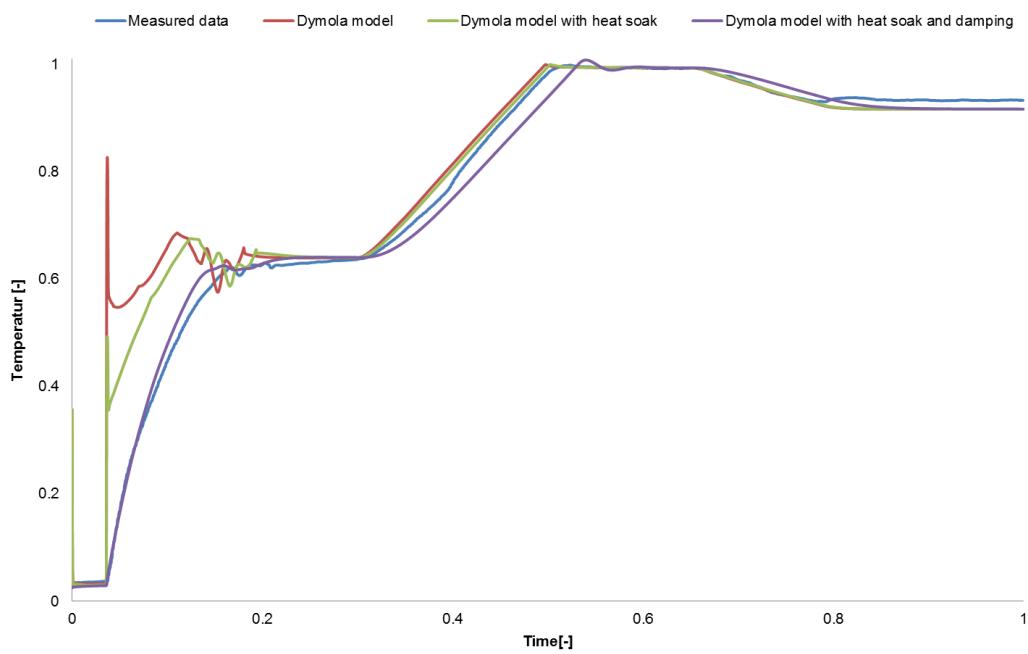
Figure 59 – Exhaust gas temperatures.

## 4.2.5 Helsingborg test conducted 2010-04-30
Start
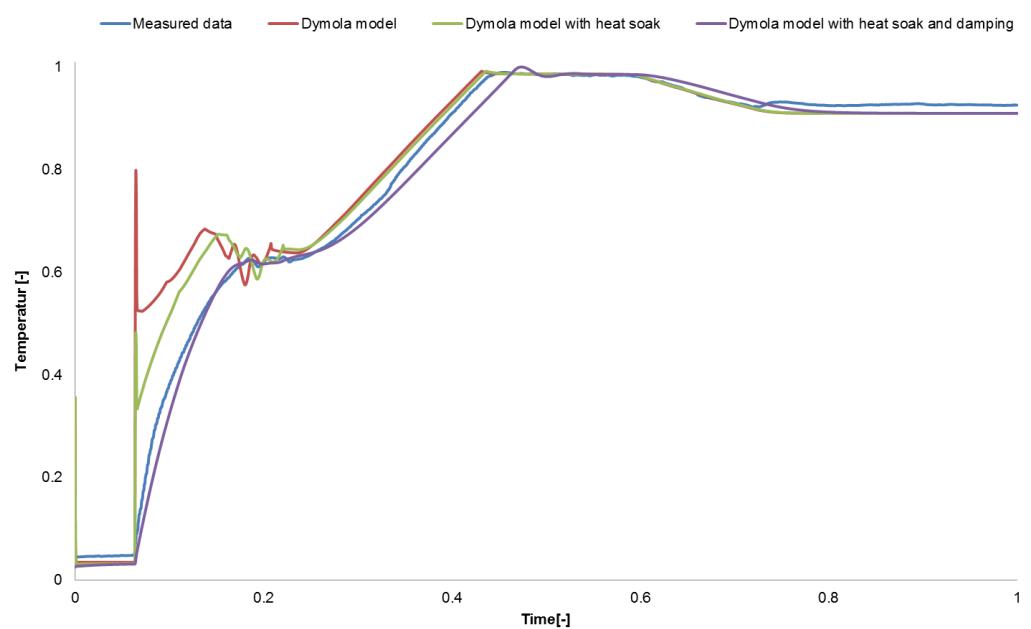
Figure 60 – Exhaust gas temperatures.

54

5 Discussion and conclusions

The objective of this project was to implement heat soak and probe inertia to the existing dynamic gas turbine model of Siemens SGT-800. It is of great interest to be able to simulate both real and probe temperatures in the gas channel to ensure customers and development projects receive correct data. Findings and problems that occurred during the project are analyzed and discussed in this section.

5.1 Validation of simulations

As illustrated in the result chapter the exhaust gas temperature accords to measured data during a start operation. The compressor outlet temperature is in a good agreement with measured data but reacts slower during transient than the exhaust gas temperature. This difference in reaction time probably occurs due to probes inertia. For the compressor outlet temperature to accord more accurate to measured data, inertia at the end of the start operation should increase without changing the inertia at the start.

The comparison of metal temperatures and gas channel temperatures clearly illustrated the amount of energy which is possible to transfer instantaneously. It also illustrates how fast a component reacts during transients.

During a stop operation both the compressor outlet temperature and the exhaust gas temperatures reacted too fast compared to measured data. Possible errors could be that the computed mass flow and the measured mass flow differ. This is indicated in figure 47. A new thermal mass that is exposed to a colder temperature or in some cases the metal temperature could be added to increase inertia in the system. By implementing inertia in the system the gas channel temperature is influenced and reacts slower.

5.2 Different reaction time for probes

During a start operation the measured exhaust gas temperature reacts faster than the compressor outlet temperature. This is illustrated in figure 37 and 38 in the result chapter. The same types of thermocouples are installed at compressor outlet and at the turbine outlet. The probes might be encapsulated in a different way or exposed to the gas flow in a different way which will affect how fast they react during transients.

5.3 Mass flow

Computed values in Dymola of the mass flow during barring speed differs from measured data. The phenomenon is illustrated figure 47. Measured data indicate zero mass flow and the computed value from Dymola indicates a mass flow of 11 kg/s. According to engineers at SIT with knowledge in the area the mass flow should have a value around 4-5 kg/s at a specific barring speed of 200 rmp. Neither of the values illustrated in figure 47 is correct but the difference has a large impact on how fast gas channel temperatures decreases during a stop operation. Computed values from Dymola are not possible to adjust due to the fact that the model crashes when the compressor mass flow turns under a certain value.

5.4 Adding an additional thermal mass

To cope with the high inertia in temperatures during a stop operation an additional thermal mass could be added to the dynamic model in Dymola. The additional mass would act as an outer part of the casing, the discs in the turbine and the inner part in the rotor of the compressor. The mass is exposed to a lower temperature which is directly affected by the temperature from the other thermal mass. During a stop

operation the metal mass transfers heat during a long period of time and therefore contributes to an increase in the inertia of the gas channel temperature. The additional metal mass would work as an independent heat soak model.

5.5 Heat soak model

One of the questions that raised during the project was the choice of size of the heat soak model. At the beginning of the project the aim was to have three models: a compressor, a combustor and a turbine. The accuracy of the models was not satisfactory as the temperature difference and the thermal mass difference between inlet and outlet were too large. A tradeoff was made between execution time and the accuracy of the heat soak model. The compressor model was divided into fifteen stages, the combustor into two parts and the turbine into three stages. To save execution time and simplify the model, the intention was to attempt to combine the heat soak models of two or more stages and analyze how the change influences the accuracy of the gas turbine model. The tradeoff between the decrease in the number of heat soak models to save execution time and accuracy have not been included in this report but is recommended for future work.

5.6 Uncertainty of probe inertia

The use of a transfer function does not intercept the physical behavior of a probe. It only mimics the behavior of the measured data. With the uncertainty of parameters such as thermal mass and heat transfer coefficient for the heat soak model. The parameters need to be tuned in. To be able to perceive the amount of inertia that the probes contribute to the gas channel temperature would be of great interest. The implementation of a heat soak model as a probe would describe the physical behavior of the probe and give the correct, measured temperature.

5.7 Earlier work

Earlier work within the subject of heat soak in gas turbines is limited and the possibility of comparing findings and results to earlier work is restricted. To ensure the accuracy of the heat transfer model and probe inertia, measured data were used. To compare the result and findings to earlier work would have given a more distinct assurance of the correctness of results and a deeper understanding of the problems which occurred during this project.

Literature where heat soak in gas turbines are discussed have been found and used in this thesis. According to Walsh and Fletcher [12] the combustor has the largest effect on heat soak due to its large surface area, thermal mass and temperature change. Results from this project demonstrate that the turbine has the largest effect. As previously mentioned, parameters such as surface area, thermal mass, temperature change and heat transfer coefficient decide the effect of heat soak. Since there are several different configurations of combustors the effect differs as well. In this project the thermal mass of the combustor was low and due to film cooling the effect of transfer heat to the encapsulating casing was negligible.

5.8 Conclusions

- Implementing heat soak and probe inertia to gas channel temperatures in the model results in good agreement to measured data during a start operation.
- Adding an additional thermal mass and configuring mass flows provide a better agreement between simulated and measured gas channel temperatures during a stop operation.

- Probe inertia has a large impact on reaction time during transient of gas channels temperatures.

5.9 Future work

The following course of action is suggested as future work:

- Implement an additional mass which is affected by a lower temperature. The additional mass will be implemented with a heat soak model with the same configuration as the existing heat soak model. Implementing an additional mass might contribute to integrating inertia to the gas channel temperature in an efficient way.

- Merge heat soak models in the compressor and turbine to save execution time and simplify the model without jeopardizing the accuracy of the results. Execution time can be saved by combining heat soak models for two or more stages and analyze how the change influence the accuracy of the gas turbine model. The tradeoff between decreasing in the amount of heat soak models to save execution time and accuracy is recommended as future work.

- Make it possible to run the Dymola model at low barring flow which decreases the difference between measured and computed mass flows. The gas turbine model has at the current moment not the possibility to decrease the mass flow to requested levels. When the mass flow decreases under the requested level the model crashes probably due to the fact that too high flows are ejected from the compressor to bleeds.

6 Bibliography

[1] ASEA-STAL [Internet]. [Place unknown]: Kulturarv Ostergotaland; 2003 [Cited 2016 March 12]. Available from:
http://www.kulturarvostergotland.se/img/html_pobfin/html/finsp_asea.html

[2] FINSPÅNG [Internet]. [Place unknown]: Kulturarv Ostergotaland; 2003 [Cited 2016 March 12]. Available from:
http://www.kulturarvostergotland.se/img/html_pobfin/html/finsp_indhi.html

[3] En historia om drivkraft [Internet]. [Place unknown]: Siemens Industrial Turbomachinery AB; 2013 [Cited 2016 March 12]. Available from: http://sit-ab.leon.se/

[4] Paris Agreement [Internet]. [Place unknown]: European Commission; [Cited 2016 March 12] Available from:
http://ec.europa.eu/clima/policies/international/negotiations/paris/index_en.htm

[5] von Wowern C. RTGRP 34/08 - Development, testing and verification of a general heat soak model for compressors. Finspång: Siemens Industrial Turbomachinery; 2008.

[6] Larsson J. RTREI035/2010 - SGT-800B. Finspång: Siemens Industrial Turbomachinery; 2010.

[7] Walsh P.P, Fletcher P. Gas turbine performance. Second edition. Oxford: Blackwell Science Ltd; 1998.

[8] Nogenmyr K.J. RT HT 033 15 - SGT-800 compressor rotor: Improved thermal boundary conditions. Finspång: Siemens Industrial Turbomachinery; 2015.

[9] Annerfeldt M.1CS13109 - Simulations of overspeeds at generator trip for the GT140P, KARITA. Finspång: Siemens Industrial Turbomachinery; 1999.

[10] Cengel Y.A, Boles M.A. Thermodynamics an engineering approach. Seventh edition. New York: McGraw-Hill; 2011.

[11] Dixon S. L, Hall C. A. Fluid Mechanics and Thermodynamics of Turbomachinery. Seventh edition. Oxford: Elsevier Inc;2014.

[12] Gudmundsson B, Nilsson U, Linder U, Shukin S, Afanasiev I, Kostege V. 98-GT-201 - Experience from the joint development of the GTX100 Turbine Blading. Finspång: Siemens Industrial Turbomachinery; 1998.

[13] Gas turbine SGT-800 [Internet]. [Place unknown]: Siemens AG; [Cited 2016 April 14]. Available from: http://www.energy.siemens.com/hq/en/fossil-power-generation/gas-turbines/sgt-800.htm#content=Description

[14] SGT-800 gas turbine [Internet]. Erlangen: Siemens AG;2014 [Cited 2016 April 14]. Available from: http://kushaindustry.com/pdf/brochure/sgt-800-gt-en.pdf

[15] Dr. Navrotsky V, Strömberg L, Uebel C. SGT-800 GAS TURBINE CONTINUED AVAILABILITY AND MAINTAINABILITY IMPROVEMENTS. Finspång: Siemens Industrial Turbomachinery; 2009.

[16] Sundén B. Värmeöverföring. Lund: Studentlitteratur; 2006.

[17] Incropera F.P, Dewitt D.P, Bergman T.L, Lavine A.S. Fundamentals of Heat and Mass Transfer. Sixth edition. New Jersey: John Wiley & Soncs, Inc; 2006.

[18] Lienhard IV J.H, Lienhard V J.H. A HEAT TRANSFER TEXTBOOK. Third edition. Cambridge, Massachusetts: Phlogiston Press; 2008.

[19] PRANDTL NUMBER [Internet]. [Place unknown]: Shires G.L; [Updated 2011 February 7; Cited 2016 May 8]. Available from: http://www.thermopedia.com/content/1053/

[20] Kumada M, Iwata S, Obata M, Watanabe O. Tip clearance effect on heat transfer and leakage flows on on the shroud-wall surface in an axial flow turbine. ASME; 1994.

[21] Hägg A, Rabal Carrera S. RT HT 004 15 - Compressor gas channel boundary condition calculations. Finspång: Siemens Industrial Turbomachinery; 2015.

[22] Jaksch P. RT_NP_027/09 - Calculation of transient heat transfer coefficients, temperature and pressures for the MGTX compressor rotor at DPL conditions. Finspång: Siemens Industrial Turbomachinery; 2009.

[23] Ekbladh E. 1CS115923 - SGT-800B Combustor, Combustor thermal loads and boundary conditions for SGT-800 B conditions. Finspång: Siemens Industrial Turbomachinery; 2013.

[24] CATIA Systems Engineering – Dymola [Internet]. [Place unknown]: DASSAULT SYSTEMS; [Cited 2016 May 9]. Available from: http://www.3ds.com/products-services/catia/products/dymola

[25] Remote Diagnostic Service for all Siemens Turbo Compressors [Internet]. [Place unknown]: Siemens AG; [Cited 2016 May 13]. Available from: http://www.energy.siemens.com/us/pool/hq/services/industrial-applications/compressors/Flyer/en/Remote%20Diagnostic%20Services%20for%20Compressors.pdf

[26] Jonsson H. PMREI009/2015 - TEMAS Export User Guide. Finspång: Siemens Industrial Turbomachinery; 2015.

[27] Filippov V. RT GRC 72/05 - GTX100 turbine version A. 2D model. Cooling of central casing, thermal calculations. Finspång: Siemens Industrial Turbomachinery; 2005.